Vertex models for the product of a permuted-basement Demazure atom and a Schur polynomial

by

Timothy Christopher Miller

A thesis
presented to the University of Waterloo
in fulfillment of the
thesis requirement for the degree of
Doctor of Philosophy
in
Combinatorics and Optimization

Waterloo, Ontario, Canada, 2026

© Timothy Christopher Miller 2026

Examining Committee Membership

The following served on the Examining Committee for this thesis. The decision of the Examining Committee is by majority vote.

External Examiner:	Ben Brubaker Professor, School of Mathematics, University of Minnesota
Supervisors:	Kevin Purbhoo Professor, Dept. of Combinatorics and Optimization, University of Waterloo
	Oliver Pechenik Assistant Professor, Dept. of Combinatorics and Optimization, University of Waterloo
Internal Member:	Olya Mandelshtam Assistant Professor, Dept. of Combinatorics and Optimization, University of Waterloo
Internal Member:	Karen Yeats Professor, Dept. of Combinatorics and Optimization, University of Waterloo
Internal-External Member:	Matthew Satriano Professor, Dept. of Pure Mathematics, University of Waterloo

Author's Declaration

I hereby declare that I am the sole author of this thesis. This is a true copy of the thesis, including any required final revisions, as accepted by my examiners.

I understand that my thesis may be made electronically available to the public.

Abstract

This thesis is about a manifestly positive combinatorial rule for the expansion of the product of two polynomials: Schur polynomials and permuted-basement Demazure atoms. Special cases of the latter polynomials include Demazure atoms and characters; there are known tableau formulas for their expansions when multiplied by a Schur polynomial, due to Haglund, Luoto, Mason and van Willigenburg [25]. We find a vertex model formula, giving a new rule even in these special cases, extending a technique introduced by Zinn-Justin [50] for calculating Littlewood–Richardson coefficients.

We derive a coloured vertex model for permuted-basement Demazure atoms. This model is inspired by Brubaker, Buciumas, Bump and Gustafsson's model for Demazure atoms [9] and Borodin and Wheeler's model for permuted-basement nonsymmetric Macdonald polynomials [8]. We make this model compatible with an uncoloured vertex model for Schur polynomials, putting them in a single framework. Unlike previous work on structure coefficients via vertex models, a remarkable feature of our construction is that it relies on a Yang–Baxter equation that only holds for certain boundary conditions. However, this restricted Yang–Baxter equation is sufficient to show our result.

Acknowledgements

I absolutely cannot thank my supervisor, Kevin Purbhoo, enough. Beyond his knowledge and insight, it would have been much harder to persevere without his boundless support and encouragement throughout my time in graduate school. Kevin gave me the space to find a foundation and grow, which enabled the deep exploration necessary for this project. I am in dismay that we were not able to continue working together until the end, due to his health issues. This in no way diminishes the recognition he deserves for fostering my research. For these reasons, I dedicate this thesis to Kevin Purbhoo.

I thank my second supervisor, Oliver Pechenik, for stepping in to advise me in Kevin's absence. Oliver had valuable feedback on this thesis as well as other important aspects of academia, which has been very helpful to me personally. I thank the other members of the committee, Ben Brubaker, Olya Mandelshtam and Karen Yeats, for valuable feedback on this thesis. I would also like to thank Per Alexandersson, Valentin Buciumas, Allen Knutson, Travis Scrimshaw and Paul Zinn-Justin for their comments on my paper that serves as the foundation of this thesis.

My affection goes out to my parents for their love and support throughout my studies. I have trouble thanking all the friends I made in graduate school, who made these the best years of my life. Any list seems to leave someone important unmentioned. So, so many of you have been special to me. If you are reading this, looking for your name, know that you are on the list and I remember.

Dedication

To Kevin Purbhoo

Table of Contents

Examining Committee ii

Author's Declaration iii

Abstract iv

Acknowledgements v

Dedication vi

List of Figures x

1 Introduction 1

1.1 Persistent definitions and notation 1

1.2 Puzzle rules and our main result 2

1.3 Schur polynomials, polynomial bases and the Schur multiplication phenomenon 5

1.4 Permuted-basement Demazure atoms 6

1.5 Vertex models 8

1.6 The Yang–Baxter equation 9

1.7 Thesis outline 10

2 Tableau Definitions and a Branching Formula **11**
2.1 Schur polynomials from SSYTs . . . 11
2.2 Permuted-basement Demazure atoms from SSAFs . . . 12
2.3 σ-extendable decompositions . . . 14

3 Previous Vertex Models **20**
3.1 Zinn-Justin's framework for the product of Schur polynomials . . . 20
3.1.1 The Schur model . . . 20
3.1.2 Vertex models for $c_{\lambda\mu}^{\nu}$ . . . 22
3.1.3 The Yang–Baxter equation . . . 24
3.1.4 Sketch of proof . . . 26
3.2 Borodin and Wheeler's model for $E_{\alpha}^{\sigma}(\mathbf{x};q,t)$ . . . 28
3.3 BBBG model for Demazure atoms . . . 31

4 Vertex Model Definitions **33**
4.1 Vertex models for atoms and Schurs . . . 33
4.2 Relating to previous vertex models . . . 36
4.3 Equivalence of atom model and skyline definition . . . 37

5 Vertex Models for $a_{\alpha\lambda}^{\beta}(\sigma)$ **44**
5.1 Theorem statement . . . 44
5.2 Proof of Theorem 5.3 . . . 46
5.3 Proof of the Column Lemma 5.8 . . . 53

6 Final Remarks **63**
6.1 Comment on the Yang–Baxter equation . . . 63
6.2 Equivariant tiles and double Demazure atoms . . . 64
6.3 Future directions . . . 66

References **68**

APPENDICES 73

A Triangle tiles and extra labels 74

List of Figures

1.1 Knutson–Tao–Woodward puzzles . . . 3
1.2 Puzzles to vertex models . . . 3
1.3 Triangular atom–Schur model . . . 4
1.4 Schematic of skyline tableau . . . 6
1.6 Polynomials of interest . . . 6
1.9 Vertices of six-vertex model . . . 8

2.1 Young diagram . . . 12
2.3 Augmented filling example . . . 13
2.4 Type A and type B triples . . . 13
2.6 Deleting 1-cells from an SSAF . . . 14

3.2 Schur polynomial tiles . . . 21
3.4 All Zinn-Justin's tiles . . . 23
3.10 Schematic of Borodin and Wheeler's model, $\sigma = \mathrm{id}$ . . . 28
3.11 Borodin and Wheeler's tiles . . . 29
3.15 Bijection between BW model and SSAFs . . . 31
3.16 Brubaker, Buciumas, Bump and Gustafsson's vertices . . . 31

4.2 Atom and Schur tiles . . . 34
4.5 Schematic of Borodin and Wheeler's model, general σ . . . 36
4.6 Borodin and Wheeler model's relationship to ours . . . 37

5.1 Diamond tiles 44
5.2 Banned adjacencies 45
5.6 All tiles 47
5.12 Proof illustration 51
5.14 Uncrossing lines 54

6.1 Tiles for the double Schur model 64

Chapter 1

Introduction

In this chapter, we state our results and place them within the context of broader literature. Section 1.1 details definitions and persistent symbols used throughout this thesis. Section 1.2 outlines structure coefficients and the history of puzzle rules, stating our main result, which is a puzzle rule. Section 1.3 and Section 1.4 cover relevant background on the Schur multiplication phenomenon and our polynomials of interest. Section 1.5 and Section 1.6 give background on vertex models and the Yang–Baxter equation. Finally, Section 1.7 outlines the structure of this thesis.

1.1 Persistent definitions and notation

Throughout, $\mathbf{x} = (x_1, \ldots, x_n)$ is a sequence of n variables where n is a positive integer and we use the notation $[n] := \{1, \ldots, n\}$. A ***weak composition*** $\alpha = (\alpha_1, \ldots, \alpha_n)$ is a sequence of nonnegative integers. Each integer α_i is the ***part*** of α at index i and the ***length*** of α is its number of parts, denoted $\text{len}(\alpha)$. The ***size*** of a weak composition is the sum of all its parts, denoted $|\alpha|$. The largest part in α is denoted $\max(\alpha)$.

In this thesis, a ***partition*** $\lambda = (\lambda_1, \ldots, \lambda_n)$ is a weak composition with parts sorted in descending order. Note that this allows parts of size 0, which we use to pad partitions when necessary. A ***permutation*** $\sigma = (\sigma(1), \ldots, \sigma(n))$ is an element of the symmetric group S_n. Two special permutations are the identity $\text{id} := (1, \ldots, n)$ and the reversing permutation $w_0 := (n, \ldots, 1)$. Everywhere in this thesis, α and β are weak compositions, λ, μ and ν are partitions, σ is a permutation, and all are assumed to be sequences of length n. We may also reverse any sequence $a = (a_1, \ldots, a_n)$ with $\overleftarrow{a} = (a_n, \ldots, a_1)$.

1.2 Puzzle rules and our main result

A central problem in algebraic combinatorics is finding combinatorial rules for the structure coefficients that appear in the product of certain polynomials. These coefficients can reveal the number of times one irreducible representation appears in the tensor product of two others in representation theory, or they can describe the cup product structure in cohomology. A classical example exhibiting both of these phenomena is the famous ***Littlewood–Richardson coefficients*** $c_{\lambda\mu}^{\nu}$, which appear in the product of two ***Schur polynomials*** $s_\lambda(\mathbf{x})$ and $s_\mu(\mathbf{x})$:

$$s_\lambda(\mathbf{x})s_\mu(\mathbf{x}) = \sum_\nu c_{\lambda\mu}^{\nu} s_\nu(\mathbf{x}),$$

where the summation is over partitions ν.

There are multiple ways to see that the coefficients $c_{\lambda\mu}^{\nu}$ are nonnegative integers. The coefficients $c_{\lambda\mu}^{\nu}$ are the multiplicities of irreducible representations of the general linear group, indexed by ν, within the tensor product of two others indexed by λ and μ. Geometrically, the coefficients $c_{\lambda\mu}^{\nu}$ are the structure constants for the cup product of two of Schubert classes in the Grassmannian. These structure constants count the number of intersection points of Schubert varieties in general position. Multiplicities and the number of intersection points are nonnegative integers and, thus, so are the coefficients $c_{\lambda\mu}^{\nu}$.

One can also compute Littlewood–Richardson coefficients by showing they count some specific combinatorial objects, giving a manifestly positive combinatorial rule. Such a rule was first described by Littlewood and Richardson [34], subsequently named the ***Littlewood–Richardson rule***. It computes the coefficients $c_{\lambda\mu}^{\nu}$ by counting the number of certain tableaux depending on the partitions λ, μ and ν.

Several alternative combinatorial rules for Littlewood–Richardson coefficients have since been described, including the ***puzzle rule*** of Knutson, Tao and Woodward [27, 28]. This rule determines Littlewood–Richardson coefficients by counting ***puzzles***, which are tilings of a triangular region with a fixed boundary encoding the partitions λ, μ and ν. Figure 1.1 displays the tiles and a possible puzzle.

Puzzles have since expanded into a fruitful area of research. They have been used to study equivariant K-theory [44, 48], d-step flag varieties (for $d \leq 4$) [11, 26, 29, 30, 31], and more recently to formulate signed puzzle rules for Schubert coefficients [43].

Retracing back to 2009, Zinn-Justin [50] connected puzzles to integrable systems by identifying them with certain statistical-mechanical models, known as ***vertex models***.

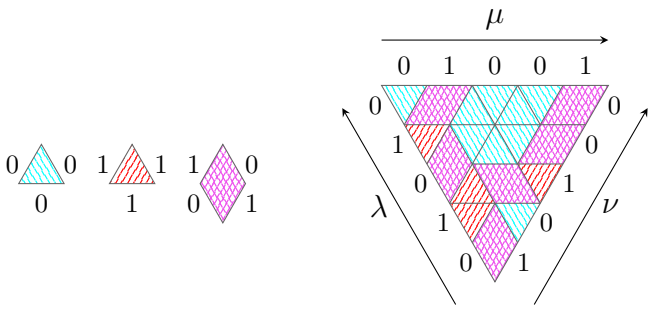


Figure 1.1: The tiles and an example of a Knutson–Tao–Woodward puzzle where $\lambda = (2, 1, 0)$, $\mu = (1, 1, 0)$ and $\nu = (2, 2, 1)$. There is one filling in this case, showing $c^{\nu}_{\lambda\mu} = 1$. Edge labels must match, and tiles may be rotated, but not reflected.

He envisioned Schur polynomials and puzzles as particle systems where two interacting species of fermions evolve in one dimension of space over time. These were then placed in a unified framework, yielding an elegant proof of the puzzle rule, which is the inspiration for this thesis. The proof works by gluing two models for Schur polynomials together, corresponding to multiplication, and then transforming them via a ***Yang–Baxter equation*** into a new picture representing a summation of Schur polynomials. Within this new image, a triangular region determines the number of specific Schur polynomials occurring in the expansion, and each way of filling this triangle corresponds to a puzzle:

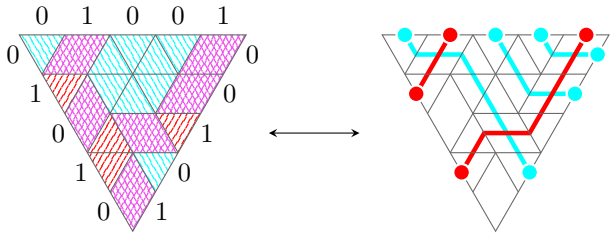


Figure 1.2: The previous puzzle and its corresponding picture in Zinn-Justin's model.

Our main result builds on this framework, giving the first combinatorial formula for the structure coefficients $a^{\beta}_{\alpha\lambda}(\sigma)$ in the product of a Schur polynomial and a ***permuted-basement Demazure atom*** $\mathcal{A}^{\sigma}_{\alpha}(\mathbf{x})$ (defined in Section 1.4):

$$\mathcal{A}^{\sigma}_{\alpha}(\mathbf{x}) s_{\lambda}(\mathbf{x}) = \sum_{\beta} a^{\beta}_{\alpha\lambda}(\sigma) \mathcal{A}^{\sigma}_{\beta}(\mathbf{x}),$$

where the summation is over weak compositions β.

Alexandersson and Sawhney [3] show the coefficients $a^{\beta}_{\alpha\lambda}(\sigma)$ are nonnegative integers and express interest in a combinatorial rule, which we now have. Our rule in Theorem 5.3 is in terms of a diamond-shaped tiling, but the top part may be discarded to give a familiar triangular rule analogous to the pictures in Figure 1.2, where the boundaries encode α, β and λ. The permutation σ has a distinguished place in the notation because it does not appear on the boundary and instead determines which crossings are allowed between blue lines:

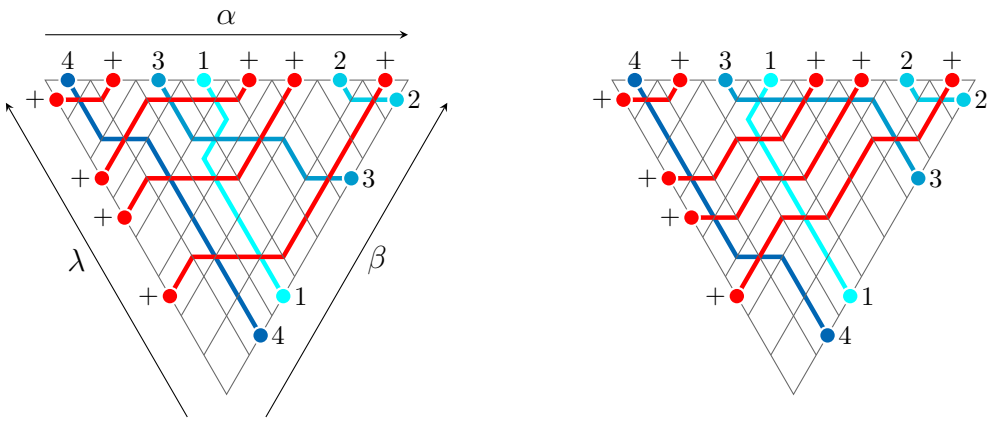


Figure 1.3: The two tilings of our model where $\alpha = (1, 3, 1, 0)$, $\beta = (1, 4, 3, 1)$ and $\lambda = (3, 1, 0, 0)$. This shows $a^{\beta}_{\alpha\lambda}(\sigma) = 2$ as long as $\sigma(1) < \sigma(3)$. If $\sigma(1) > \sigma(3)$, the crossing between lines 1 and 3 is not legal and $a^{\beta}_{\alpha\lambda}(\sigma) = 0$.

It should be stated that Figure 1.2 displays a simpler rule than originally described in [50]. Zinn-Justin's results include an extra "equivariant" tile, which we have omitted. These more general puzzles correspond to equivariant cohomology, yielding the structure coefficients for the more general double Schur polynomials $s_\lambda(\mathbf{x}, \mathbf{y})$, which are defined on two sets of variables. It is tempting to define a notion of "double" Demazure atoms in two sets of variables, analogous to double Schur polynomials. We can do this; however, our approach does not find a rule for the structure coefficients in this case. In particular, our key Yang–Baxter equation Lemma 5.8 does not hold when introducing the new set of variables analogously; see Section 6.2.

1.3 Schur polynomials, polynomial bases and the Schur multiplication phenomenon

Schur polynomials are an important basis of the ring of symmetric polynomials in n variables $\mathbb{Z}[x_1, \ldots, x_n]^{S_n}$. They are widely studied in algebraic combinatorics and have applications in representation theory and algebraic geometry. In representation theory, Schur polynomials are the characters of irreducible representations of the general linear group. They also play an important role in the representation theory of the symmetric group. Geometrically, Schur polynomials represent the cohomology classes of Schubert varieties in Grassmannians. We give the combinatorial description of Schur polynomials in terms of semistandard Young Tableaux in Section 2.1. They may also be obtained as specializations of the polynomials $\mathcal{A}^{\sigma}_{\alpha}(\mathbf{x})$.

For a fixed permutation $\sigma \in S_n$, the set $\{\mathcal{A}^{\sigma}_{\alpha}(\mathbf{x})\}_{\alpha}$, where α ranges over all weak compositions of length n, is a basis of the polynomial ring $\mathbb{Z}[x_1, \ldots, x_n]$. Two well-studied special cases of the polynomials $\mathcal{A}^{\sigma}_{\alpha}(\mathbf{x})$ are ***Demazure atoms*** $\mathcal{A}_{\alpha}(\mathbf{x})$ ($\sigma = \mathrm{id}$) and ***Demazure characters*** $\mathcal{K}_{\alpha}(\mathbf{x})$ ($\sigma = w_0$). Some conventions may reverse the order of α on either side of these definitions; see Note 1.5.

Demazure characters, also called key polynomials, were introduced by Demazure [18] and studied combinatorially by Lascoux and Schützenberger [33]. They are characters of representations of a Borel subgroup, known as Demazure modules, and they generalize Schur polynomials. In our conventions, we have $\mathcal{K}_{\lambda}(\mathbf{x}) = s_{\lambda}(\mathbf{x})$ when λ is a partition. Demazure characters are also a special case of Kohnert polynomials, introduced by Assaf and Searles [5]. There are some interesting open problems regarding expansions of these polynomials; for instance, it is conjectured that the product of two characters expands positively in the Demazure atom basis; see Pun [45].

Many other bases of the polynomial ring are known to expand positively in that same basis when multiplied by a Schur polynomial; see Searles [46] for detailed discussion. Haglund, Luoto, Mason and van Willigenburg [25] give positive rules for the products of a Schur polynomial with a Demazure atom or character, expressed in terms of certain tableaux known as skyline fillings; see also Assaf [4]. Our result yields new rules even in these special cases. The author's work in a FPSAC extended abstract for this thesis [38] originally considered two separate models for Demazure atoms and characters. Now both are captured by one framework, where setting $\sigma = \mathrm{id}$ gives the rule for atoms and $\sigma = w_0$ yields the rule for characters. The main work of this thesis is also available in a preprint [39].

1.4 Permuted-basement Demazure atoms

Permuted-basement Demazure atoms $\mathcal{A}^{\sigma}_{\alpha}(\mathbf{x})$ are the $q = t = 0$ specializations of ***permuted-basement nonsymmetric Macdonald polynomials*** $E^{\sigma}_{\alpha}(\mathbf{x}; q, t)$, introduced in 2011 by Ferreira [20]; two sources of further exposition are Alexandersson [2] and Guo and Ram [23]. These polynomials are generalizations of ***nonsymmetric Macdonald polynomials*** $E_{\alpha}(\mathbf{x}; q, t)$, which are the case where $\sigma = w_0$. Haglund, Haiman and Loehr [24] gave a combinatorial formula for $E_{\alpha}(\mathbf{x}; q, t)$ in terms of "skyline" tableaux which contain a permutation σ in the bottom row, which has become known as the basement; their permuted-basement versions, hence, permute this basement:

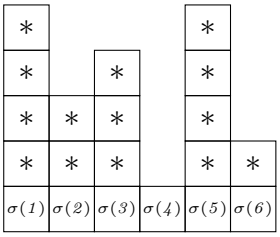


Figure 1.4: Schematic of a skyline tableau of shape $\alpha = (4, 2, 3, 0, 4, 1)$ with basement σ. The boxes marked with $*$ are filled with integers according to certain rules, left unspecified.

Note 1.5. We use conventions for $\mathcal{A}^{\sigma}_{\alpha}(\mathbf{x})$ and $E^{\sigma}_{\alpha}(\mathbf{x}; q, t)$ that align with Alexandersson [2], setting $\mathcal{A}^{\sigma}_{\alpha}(\mathbf{x}) := E^{\sigma}_{\alpha}(\mathbf{x}; 0, 0)$. Again, some conventions in the literature may reverse the order of α; in particular, the conventions in [24] for $E_{\alpha}(\mathbf{x}; q, t)$ reverse the order of α. The following diagram summarizes the relationship between polynomials mentioned thus far, according to our conventions:

$$\begin{array}{ccccc} E^{\sigma}_{\alpha}(\mathbf{x}; q, t) & \xrightarrow{q=t=0} & \mathcal{A}^{\sigma}_{\alpha}(\mathbf{x}) & \xrightarrow{\sigma=\mathrm{id}} & \mathcal{A}_{\alpha}(\mathbf{x}) \\ \downarrow{\scriptstyle \sigma=w_0} & & \downarrow{\scriptstyle \sigma=w_0} & & \\ E_{\alpha}(\mathbf{x}; q, t) & \xrightarrow{q=t=0} & \mathcal{K}_{\alpha}(\mathbf{x}) & \xrightarrow{\alpha=\lambda} & s_{\lambda}(\mathbf{x}) \end{array}$$

Figure 1.6: Connection between our polynomials of interest.

Nonsymmetric Macdonald polynomials were introduced simultaneously in a series of papers by Cherednik [14, 15], Macdonald [35] and Opdam [41]. Cherednik defined them as the unique simultaneous eigenfunctions of what have become known as Cherednik–Dunkl operators, which are generators of an abelian subalgebra of the Double Affine Hecke

algebra. Cherednik used these polynomials and operators to prove Macdonald's constant term conjecture for Macdonald polynomials [14].

Permuted-basement nonsymmetric Macondald polynomials may be obtained through applying generators of the Affine Heck algebra, known as Demazure–Lusztig operators, to a nonsymmetric Macdonald polynomial. Combinatorially, these operators permute the basement; this was stated in [20] and proved in [2]. We present the $q = t = 0$ case, determining the polynomials $\mathcal{A}^{\sigma}_{\alpha}(\mathbf{x})$.

A simple transposition $s_i = (i, i+1)$ is the permutation that swaps i and $i+1$. The ***Coxeter length*** $\ell(\sigma)$ of a permutation σ is the minimum number of simple transpositions needed to generate σ. A ***reduced word*** for a permutation σ is a string of simple transpositions $s_{i_1} \cdots s_{i_k}$ that generates σ. We define the following operators:

$$\partial_i = \frac{1 - s_i}{x_i - x_{i+1}}, \qquad \pi_i = \partial_i x_i, \qquad \theta_i = \pi_i - 1.$$

We must first determine the case where $\sigma = \mathrm{id}$, which is the Demazure atom $\mathcal{A}_{\alpha}(\mathbf{x})$. For a partition λ, let $\mathbf{x}^{\lambda} = x_1^{\lambda_1} \cdots x_n^{\lambda_n}$. For a reduced word $w = w_1 \cdots w_k$ for τ, define $\theta_w = \theta_{w_1} \cdots \theta_{w_k}$. Let λ be the partition with the same parts as α and let τ be a minimal length permutation such that $\tau(\lambda) = (\lambda_{\tau^{-1}(1)}, \ldots, \lambda_{\tau^{-1}(n)})) = \alpha$. The Demazure atom $\mathcal{A}_{\alpha}(\mathbf{x})$ is given by

$$\mathcal{A}_{\alpha}(\mathbf{x}) := \theta_w \mathbf{x}^{\lambda}.$$

Example 1.7. Let $\alpha = (1, 0, 1, 3)$ so that $\tau(\lambda) = \alpha$, where $\lambda = (3, 1, 1, 0)$ and $\tau = (4, 1, 3, 2)$. Then $w = s_2 s_3 s_2 s_1$ is a reduced word for τ. We compute

$$\mathcal{A}_{\alpha}(\mathbf{x}) = \theta_w \mathbf{x}^{\lambda} = x_1^2 x_3 x_4^2 + x_1 x_2 x_3 x_4^2 + x_1 x_3^2 x_4^2 + x_1 x_3 x_4^3.$$

Next, we permute the basement σ using proposition 15 of [2] (note that Alexandersson uses right multiplication notation to mean what we do with left multiplication). We have the choice of using either π_i to decrease the length of σ or θ_i to increase the length. Let $\gamma_i = \alpha_{\sigma^{-1}(i)}$; this corresponds to the size of the part sitting above the basement entry i in a skyline tableau. If $\ell(\sigma s_i) < \ell(\sigma)$, we have

$$\theta_i \mathcal{A}^{\sigma}_{\alpha}(\mathbf{x}) = \mathbf{1}_{\gamma_i > \gamma_{i+1}} \times \mathcal{A}^{s_i \sigma}_{\alpha}(\mathbf{x}),$$

where $\mathbf{1}$ is the indicator function. If $\ell(\sigma s_i) < \ell(\sigma)$, we have

$$\pi_i \mathcal{A}^{\sigma}_{\alpha}(\mathbf{x}) = \mathbf{1}_{\gamma_i \geq \gamma_{i+1}} \times \mathcal{A}^{s_i \sigma}_{\alpha}(\mathbf{x}).$$

Example 1.8. We have computed $\mathcal{A}_\alpha(\mathbf{x})$ when $\alpha = (1, 0, 1, 3)$ in the previous example. We can only increase the length of $\sigma = \mathrm{id}$. In this case, $\gamma_1 > \gamma_2$ and $\gamma_2 < \gamma_3 < \gamma_4$, so we only need to consider applying s_1. We compute

$$\mathcal{A}_\alpha^{s_1}(\mathbf{x}) = \pi_1 \mathcal{A}_\alpha(\mathbf{x}) = x_1^2 x_3 x_4^2 + 2x_1 x_2 x_3 x_4^2 + x_1 x_3^2 x_4^2 + x_1 x_3 x_4^3 + x_2^2 x_3 x_4^2 + x_2 x_3^2 x_4^2 + x_2 x_3 x_4^3.$$

Let $\alpha = (1, 0, 3, 1)$ and $\sigma = (4, 2, 1, 3)$, in which case we have $\mathcal{A}_\alpha^\sigma(\mathbf{x}) = x_1^3 x_3 x_4$. Here, we have $(\gamma_1, \gamma_2, \gamma_3, \gamma_4) = (3, 0, 1, 1)$, so $\gamma_1 > \gamma_2$ and $\gamma_2 < \gamma_3 = \gamma_4$. We have that $s_1\sigma = (4, 1, 2, 3)$ and $\ell(s_1\sigma) < \ell(\sigma)$, so we may apply θ_1 to compute

$$\mathcal{A}_\alpha^{s_1\sigma}(\mathbf{x}) = \theta_1 \mathcal{A}_\alpha^\sigma(\mathbf{x}) = x_1^2 x_2 x_3 x_4 + x_1 x_2^2 x_3 x_4 + x_2^3 x_3 x_4.$$

We may also verify that $\ell(s_2\sigma) > \ell(\sigma)$, $\ell(s_3\sigma) < \ell(\sigma)$ and $\pi_2 \mathcal{A}_\alpha^\sigma(\mathbf{x}) = \theta_3 \mathcal{A}_\alpha^\sigma(\mathbf{x}) = 0$.

1.5 Vertex models

Vertex models are a tool developed in statistical mechanics to study particle systems. A notable example is the six-vertex or square-ice model, which has vertices commonly depicted as in Figure 1.9. Vertices are arranged within a lattice, often with a fixed boundary, and each vertex is assigned a weight depending on its bonds with its neighbours. A total weight is calculated for any given arrangement of the entire lattice by multiplying the weights of all its individual vertices. The sum of all these weights over all possible configurations is the ***partition function*** of the model.

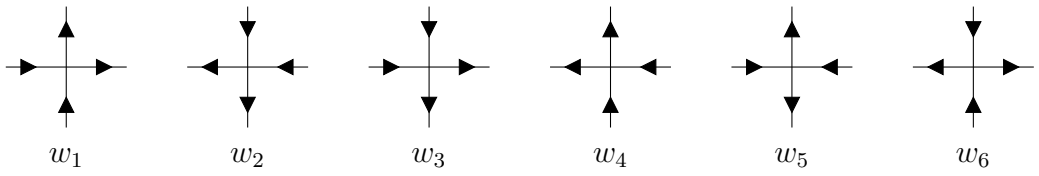


Figure 1.9: Vertices of the six-vertex model with weights $w_1, \ldots, w_6$.

Vertex models have led to major advances in algebraic combinatorics, with many recent results demonstrating their applicability. Families of polynomials studied via vertex models include double Schur polynomials [50], Grothendieck polynomials [10, 22, 40, 48], LLT polynomials [16, 17], some versions of Macdonald polynomials [1, 8, 21], Demazure atoms and characters [9, 12] and Lascoux polynomials [13]. Other applications include puzzle

rules [29, 30, 31, 48, 50], Cauchy identities [6, 7, 22, 47] and branching formulas [7, 10, 19, 22].

An advantage of formulating a problem in terms of vertex models is that it can lead to conceptually simple or visual proofs of identities, which we employ considerably in this thesis. Often, an important polynomial can be realized as the partition function of a vertex model with an underlying ***Yang–Baxter equation*** that makes the model amenable to analysis. However, vertex model frameworks can be rigid, depend on boundary conditions, and techniques for one may not be applicable to others.

Our polynomials of interest have already been studied in the vertex model setting. Our model for $\mathcal{A}^{\sigma}_{\alpha}(\mathbf{x})$ in Section 4.1 is originally inspired by Borodin and Wheeler's model for $E^{\sigma}_{\alpha}(\mathbf{x}; q, t)$ [8], but we make significant modifications; see Section 3.2 for Borodin and Wheeler's model and Section 4.2 for comparison with ours. Our model now bears more resemblance to the model for Demazure atoms given by Brubaker, Buciumas, Bump and Gustafsson [9]; see Section 3.3.

Vertex models also provide elegant frameworks for deriving certain recursive decompositions of special functions, known as ***branching formulas***. We prove a branching formula for the polynomials $\mathcal{A}^{\sigma}_{\alpha}(\mathbf{x})$, which is Theorem 2.11. We use this to show our vertex models yield the correct polynomials. Building up to this statement, we derive a partial order for weak compositions, which could be the subject of future work.

Another potential drawback of the vertex model approach is that the Yang–Baxter equation is a strong requirement that could be hard to find or may not exist. It is often the case that vertex models are constructed from **R-*matrices*** that satisfy the Yang–Baxter equation, in which case they are called ***integrable*** or ***solvable***. Our situation is unusual in that our Yang–Baxter equation, Lemma 5.8, only holds for certain boundary conditions. Fortunately, these restrictions are satisfied when needed. Other cases involve going beyond the Yang–Baxter equation in a more fundamental way. For instance, Buciumas and Scrimshaw [12] find that one of their anticipated Yang–Baxter equations does not hold when considering Demazure atoms and characters in type B and C, but a different relation allows them to characterize their partition functions. Zhong [49] finds a similar phenomenon in stochastic type C vertex models.

1.6 The Yang–Baxter equation

Let V be a vector space, $\mathbf{I}$ be the identity matrix acting on V, and $\mathbf{R}$ be a matrix acting on $V \otimes V$, referred to as an $\mathbf{R}$-matrix. In its most basic form, we say $\mathbf{R}$ satisfies the

Yang–Baxter equation if

$$(\mathbf{R}\otimes\mathbf{I})(\mathbf{I}\otimes\mathbf{R})(\mathbf{R}\otimes\mathbf{I}) = (\mathbf{I}\otimes\mathbf{R})(\mathbf{R}\otimes\mathbf{I})(\mathbf{I}\otimes\mathbf{R}).$$

The $\mathbf{R}$-matrices may also contain parameters, in which case the Yang–Baxter equation may be written

$$(\mathbf{R}(x)\otimes\mathbf{I})(\mathbf{I}\otimes\mathbf{R}(z))(\mathbf{R}\otimes\mathbf{I}(y)) = (\mathbf{I}\otimes\mathbf{R}(y))(\mathbf{R}(z)\otimes\mathbf{I})(\mathbf{I}\otimes\mathbf{R}(x)).$$

This version is called the ***parameter-dependent*** Yang–Baxter equation. The parameters x, y, z usually satisfy some relationship such as $x+y=z$ or $x+y+z=0$. $\mathbf{R}$-matrices may also have a check, denoted $\check{\mathbf{R}}$, indicating that they act by $\mathbf{R}$ and then swap the objects. Further, there are two different versions the Yang–Baxter equation that may use the notation $\mathbf{R}_{ab}$ where $a, b \in \{1,2,3\}$ to indicate $\mathbf{R}$ is acting on objects in positions a and b:

$$\mathbf{R}_{12}\mathbf{R}_{13}\mathbf{R}_{23} = \mathbf{R}_{23}\mathbf{R}_{13}\mathbf{R}_{12},$$
$$\mathbf{R}_{23}\mathbf{R}_{12}\mathbf{R}_{23} = \mathbf{R}_{12}\mathbf{R}_{23}\mathbf{R}_{12}.$$

These versions may also be parameter-dependent. See Section 3.1.3 for a full example of a parameter-dependent Yang–Baxter equation where the $\mathbf{R}$-matrices come from Zinn-Justin's vertex model [50].

1.7 Thesis outline

In Chapter 2, we give the tableau definitions of $s_\lambda(\mathbf{x})$ and $\mathcal{A}^\sigma_\alpha(\mathbf{x})$ and derive a branching formula in Theorem 2.11. One may skip Section 2.3 unless they are interested in the branching formula or need details of the proof of our model's correctness. Chapter 3 provides exposition on Zinn-Justin's framework and previous vertex models that we build on. Chapter 4 defines our vertex models for $\mathcal{A}^\sigma_\alpha(\mathbf{x})$ and proves they have the correct definition in Theorem 4.10. We prove our main Theorem 5.3 in Chapter 5. Chapter 6 has final remarks and suggestions for future directions.

Chapter 2

Tableau Definitions and a Branching Formula

This chapter gives combinatorial definitions for Schur polynomials and permuted-basement Demazure atoms, which are found in Section 2.1 and Section 2.2. In Section 2.3, we define the σ-extendable relation, a notion we use in the definition of a covering relation on weak compositions. We then derive the branching formula in Theorem 2.11 for permuted-basement Demazure atoms, written as a sum over saturated chains in the resulting poset. Theorem 2.11 is used in Section 4.3 of the next chapter to show our vertex models describe the same polynomials.

2.1 Schur polynomials from SSYTs

A ***Young diagram*** of ***shape*** λ is a box diagram representing the partition $\lambda = (\lambda_1, \ldots, \lambda_n)$. In the English convention, each row represents a part λ_i of the partition and rows weakly decrease in length from top to bottom:

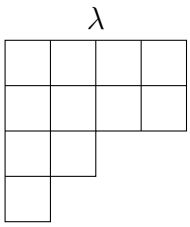


Figure 2.1: A Young diagram of shape $\lambda = (5, 5, 2, 1)$.

A ***semistandard Young tableau*** is a filling of a Young diagram with positive integers that weakly increase across rows and strictly increase down columns. Let $\mathrm{SSYT}_n(\lambda)$ denote the set of all semistandard Young tableaux of shape λ where the largest entry in the filling is n. We define the ***Schur polynomial*** $s_\lambda(\mathbf{x})$ as a summation over semistandard Young tableaux:

$$s_\lambda(\mathbf{x}) = \sum_{T \in \mathrm{SSYT}_n(\lambda)} \mathbf{x}^T,$$

where $\mathbf{x}^T$ is a monomial $\prod_{i=1}^{n} x_i^{t_i}$ such that t_i counts the number of entries i in a particular tableau T.

Example 2.2. When $\lambda = (2, 2, 1)$ and $n = 3$, there are three fillings in $\mathrm{SSYT}_n(\lambda)$:

1	1
2	2
3	

1	1
2	3
3	

1	2
2	3
3	

This shows that $s_\lambda(\mathbf{x}) = x_1^2 x_2^2 x_3 + x_1^2 x_2 x_3^2 + x_1 x_2^2 x_3^2$.

2.2 Permuted-basement Demazure atoms from SSAFs

In this section, we define permuted-basement Demazure atoms in terms of the semi-skyline augmented fillings, introduced by Mason [36, 37]. We first introduce several notions that go into the definition.

For a weak composition α, an ***augmented filling*** of ***shape*** α is a function that assigns positive integers to a tableau representing α:

$$F : \{(i, j) \mid i \in [n], 0 \leq j \leq \alpha_i\} \to \mathbb{Z}_+.$$

The pairs (i, j) in the domain of F are called the ***cells***; we write $F((i, j)) := F(i, j)$ as shorthand. We say that a cell is in F if it is in the domain of F. The ***entry*** of a cell c is the value $F(c)$ and a cell with entry e is an *e*-***cell*** of F. We say a permutation σ is the ***basement*** of F if $F(i, 0) = \sigma(i)$ for all $i \in [n]$. We depict augmented fillings with diagrams as in the figure below:

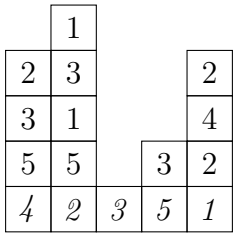


Figure 2.3: An augmented filling of shape $\alpha = (3, 4, 0, 1, 3)$ with basement $\sigma = (4, 2, 3, 5, 1)$.

A ***descent*** of F is a pair of cells (i, j) and $(i, j + 1)$ for $i \in [n]$ and $j \geq 0$, where $F(i, j) < F(i, j + 1)$. In other words, a descent is a pair of adjacent cells in F that are assigned decreasing entries read from top to bottom.

We specify two types of "triples" that can occur in an augmented filling; let $1 \leq \ell < r \leq n$. If $\alpha_\ell \geq \alpha_r$, we say a ***type A triple*** within columns ℓ and r is of the form $\{(\ell, i + 1), (r, i + 1), (\ell, i)\}$ for $0 \leq i < \alpha_r$. If $\alpha_\ell < \alpha_r$, a ***type B triple*** within columns ℓ and r is of the form $\{(r, i + 1), (\ell, i), (r, i)\}$ for $0 \leq i \leq \alpha_\ell$. Note that both triples and descents can include basement cells. The following schematic illustrates triples, labelling cells with their entries a, b and c:

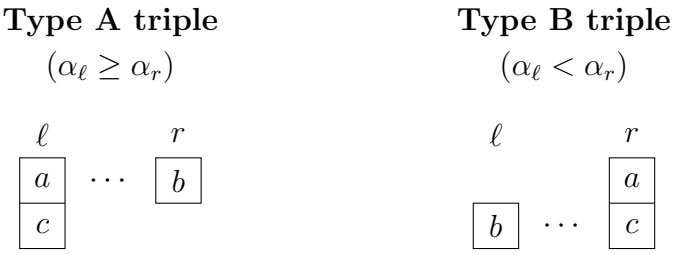


Figure 2.4: Type A and type B triples within columns ℓ and r.

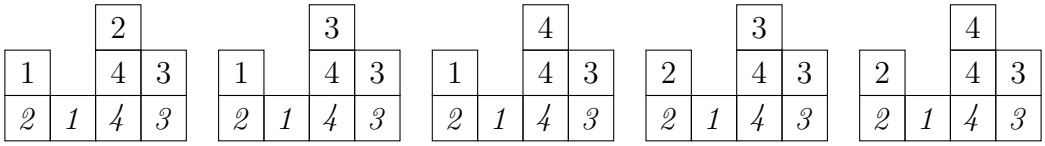
In either case, we say a triple is ***inversion*** if $b \notin [a, c]$ and ***coinversion*** if $b \in [a, c]$. A ***semi-skyline augmented filling (SSAF)*** F is an augmented filling with no descents

where all triples are inversion triples. Denote the set of all SSAFs of shape α with basement σ by $\mathrm{SSAF}_\sigma(\alpha)$. Finally, the polynomials $\mathcal{A}^\sigma_\alpha(\mathbf{x})$ are given by a summation over all fillings in $\mathrm{SSAF}_\sigma(\alpha)$:

$$\mathcal{A}^\sigma_\alpha(\mathbf{x}) = \sum_{F \in \mathrm{SSAF}_\sigma(\alpha)} \mathbf{x}^F,$$

where $\mathbf{x}^F$ is the product $\prod_c x_{F(c)}$ over all **non-basement** cells c in F.

Example 2.5. When $\alpha = (1, 0, 2, 1)$ and $\sigma = (2, 1, 4, 3)$, there are five fillings in $\mathrm{SSAF}_\sigma(\alpha)$:



This shows that $\mathcal{A}^\sigma_\alpha(\mathbf{x}) = x_1x_2x_3x_4 + x_1x_3^2x_4 + x_1x_3x_4^2 + x_2x_3^2x_4 + x_2x_3x_4^2$. We emphasize again that the basement entries in F do not contribute to a given monomial $\mathbf{x}^F$.

2.3 σ-extendable decompositions

In this section, we prove a branching formula for permuted-basement Demazure atoms so that we may later show that our models satisfy the same branching formula in Section 4.3. This section may be skipped if the reader is not interested in the branching formula or details of the proof in Section 4.3. The key insight, which entails Lemma 2.9, is that removing all non-basement 1-cells from a filling in $\mathrm{SSAF}_\sigma(\alpha)$ yields another filling in $SSAF_\sigma(\beta)$ for some β. We say that all such β are σ-extendable to α. Then $\mathcal{A}_\alpha(\mathbf{x})$ may be written as a sum over all β that are σ-extendable to α.

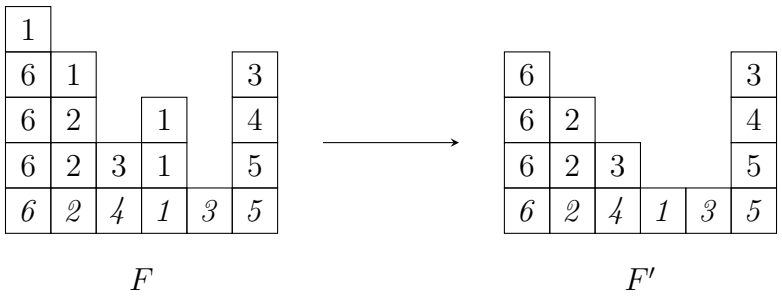


Figure 2.6: Deleting non-basement 1-cells from an SSAF.

Definition 2.7. Given weak compositions α and β of length n and $\sigma \in S_n$, we say that β is ***σ-extendable*** to α if $\alpha_i \geq \beta_i$ for $i \in [n]$ and the following conditions hold for each pair (ℓ, r) satisfying $1 \leq \ell < r \leq n$:

1. If $\alpha_\ell \geq \alpha_r$ and $\beta_\ell \geq \beta_r$, then $\alpha_r \leq \beta_\ell$.
2. If $\alpha_\ell < \alpha_r$ and $\beta_\ell < \beta_r$, then $\alpha_\ell < \beta_r$.
3. If $\alpha_\ell \geq \alpha_r$ and $\beta_\ell < \beta_r$, then $\alpha_r = \beta_r$ and $\sigma(\ell) < \sigma(r)$.
4. If $\alpha_\ell < \alpha_r$ and $\beta_\ell \geq \beta_r$, then $\alpha_\ell = \beta_\ell$ and $\sigma(\ell) > \sigma(r)$.

In Figure 2.6, F has shape $\alpha = (4, 3, 1, 2, 0, 3)$, F' has shape $\beta = (3, 2, 1, 0, 0, 3)$, $\sigma = (6, 2, 4, 1, 3, 5)$ and we have that β is is σ-extendable to α. We make use of the next lemma to clean up the proof of Lemma 2.9; one may also verify that the lemma holds for F and F'.

Lemma 2.8. *Let $F \in \mathrm{SSAF}_\sigma(\alpha)$, where α and σ have length n, and let $1 \leq \ell < r \leq n$.*

1. *If $\alpha_\ell \geq \alpha_r$ and $0 \leq a \leq \alpha_r$, then:*
   (a) *If $F(\ell, a) < F(r, a)$, then $F(\ell, i) < F(r, i+1)$ for all $0 \leq i \leq a-1$.*
   (b) *If $F(\ell, a) > F(r, a)$, then $F(\ell, i) > F(r, i)$ for all $a \leq i \leq \alpha_r$.*
2. *If $\alpha_\ell < \alpha_r$ and $0 \leq a \leq \alpha_\ell$, then:*
   (a) *If $F(\ell, a) < F(r, a)$, then $F(\ell, i) < F(r, i+1)$ for all $a \leq i \leq \alpha_\ell$.*
   (b) *If $F(\ell, a) > F(r, a)$, then $F(\ell, i) > F(r, i)$ for all $0 \leq i \leq a$.*

Proof. 1. Assume $\alpha_\ell \geq \alpha_r$ and $0 \leq a \leq \alpha_r$.

(a) Suppose $F(\ell, a) < F(r, a)$. If $a = 0$, the inequality is vacuously satisfied. Otherwise, if $F(\ell, a-1) \geq F(r, a)$, then $\{(\ell, a), (r, a), (\ell, a-1)\}$ is a type A coinversion triple, so $F(\ell, a-1) < F(r, a)$. Then by the descent condition, $F(\ell, a-1) < F(r, a-1)$ and by induction, we have $F(\ell, i) < F(r, i+1)$ for all $0 \leq i \leq a-1$.

(b) Suppose $F(\ell, a) > F(r, a)$. If $a = \alpha_r$, we are done. Otherwise, if $F(\ell, a+1) \leq F(r, a+1)$, then $\{(\ell, a+1), (r, a+1), (\ell, a)\}$ is a type A coinversion triple, so $F(\ell, a+1) > F(r, a+1)$. By induction, we have $F(\ell, i) > F(r, i)$ for all $a \leq i \leq \alpha_r$.

2. Assume $\alpha_\ell < \alpha_r$ and $0 \le a \le \alpha_\ell$.

   (a) Suppose $F(\ell, a) < F(r, a)$. If $F(\ell, a) \ge F(r, a+1)$ then $\{(r, a+1), (\ell, a), (r, a)\}$ is a type B coinversion triple, so $F(\ell, a) < F(r, a+1)$. If $a = \alpha_\ell$, we are done; otherwise, $F(\ell, a+1) < F(r, a+1)$ by the descent condition and by induction, we have $F(\ell, i) < F(r, i+1)$ for all $a \le i \le \alpha_\ell$.

   (b) Suppose $F(\ell, a) > F(r, a)$. If $a = 0$, we are done; otherwise, $F(\ell, a-1) \ge F(\ell, a) > F(r, a)$ and thus $F(\ell, a-1) > F(r, a-1)$, since otherwise $\{(r, a), (\ell, a-1), (r, a-1)\}$ is a type B coinversion triple. By induction, we have $F(\ell, i) > F(r, i)$ for all $0 \le i \le a$.

□

We prove that the atoms $\mathcal{A}^\sigma_\alpha(\mathbf{x})$ decompose into a summation over compositions β that are σ-extendable to α. Each such β is the shape of an SSAF that remains after deleting the non-basement 1-cells from a filling in $\mathrm{SSAF}_\sigma(\alpha)$.

Lemma 2.9. *For a weak composition α of length n and $\sigma \in S_n$, we have*

$$\mathcal{A}^\sigma_\alpha(\mathbf{x}) = \sum_{\beta \ \sigma\text{-extendable to } \alpha} x_1^{|\alpha|-|\beta|} \mathcal{A}^\sigma_\beta(0, x_2, \ldots, x_n).$$

Proof. For any filling $F \in \mathrm{SSAF}_\sigma(\alpha)$, we produce a new augmented filling F' obtained by deleting all non-basement 1-cells. This augmented filling has the same basement; suppose it has shape β.

We first show that every such β is σ-extendable to α and that F' is in $\mathrm{SSAF}_\sigma(\beta)$. It is clear that $\alpha_i \ge \beta_i$ for all $i \in [n]$, so we need to check the remaining conditions of Definition 2.7 for each pair of columns and verify that the relevant triples are inversion; let $1 \le \ell < r \le n$.

1. Assume $\alpha_\ell \ge \alpha_r$ and $\beta_\ell \ge \beta_r$. If $\alpha_r > \beta_\ell$, then cells $(\ell, \beta_\ell + 1)$ and $(r, \beta_\ell + 1)$ both exist in F and have entry 1, yielding a type A coinversion triple in F, so we have $\alpha_r \le \beta_\ell$. All type A triples within columns ℓ and r in F' are inversion by assumption.

2. Assume $\alpha_\ell < \alpha_r$ and $\beta_\ell < \beta_r$. If $\alpha_\ell \ge \beta_r$, then cells (ℓ, β_r) and $(r, \beta_r + 1)$ both exist in F and have entry 1, yielding a type B coinversion triple in F, so we have $\alpha_\ell < \beta_r$. All type B triples within columns ℓ and r in F' are inversion by assumption.

3. Assume $\alpha_\ell \geq \alpha_r$ and $\beta_\ell < \beta_r$. If $\alpha_r > \beta_r$, then cells (ℓ, β_r+1) and (r, β_r+1) both exist in F and have entry 1, yielding a type A coinversion triple in F, so we have $\alpha_r = \beta_r$. It is also true that the cell (ℓ, β_r) exists in F and has entry 1, so $F(\ell, \beta_r) < F(r, \beta_r)$ and, by case 1a of Lemma 2.8, we have $F(\ell, i) < F(r, i+1) \leq F(r, i)$ for all $0 \leq i \leq \beta_r - 1$, which implies $\sigma(\ell) < \sigma(r)$ and also that all type B triples within columns ℓ and r in F' are inversion.

4. Assume $\alpha_\ell < \alpha_r$ and $\beta_\ell \geq \beta_r$. If $\alpha_\ell > \beta_\ell$, then cells $(\ell, \beta_\ell + 1)$ and $(r, \beta_\ell + 2)$ both exist in F and have entry 1, yielding a type B coinversion triple in F, so we have $\alpha_\ell = \beta_\ell$. It is also true that the cell $(r, \beta_\ell + 1)$ exists in F and has entry 1. Note that $F(\ell, \beta_\ell) > 1$ unless (ℓ, β_ℓ) is the 1-cell in the basement, but this is not possible since then we have a type B coinversion triple in F. Thus, $F(\ell, \beta_\ell) > F(r, \beta_\ell + 1)$, which entails $F(\ell, \beta_\ell) > F(r, \beta_\ell)$ since otherwise we have a type B coinversion triple in F. By case 2b of Lemma 2.8, we have $F(\ell, i) > F(r, i)$ for all $0 \leq i \leq \beta_\ell$, which implies $\sigma(\ell) > \sigma(r)$ and also that all type A triples within columns ℓ and r in F' are inversion.

Conversely, for each β that is σ-extendable to α, each filling $F' \in \mathrm{SSAF}_\sigma(\beta)$ with no 1-cells (other than the basement) may be extended to a filling F by adding $\alpha_i - \beta_i$ 1-cells above each column $i \in [n]$ in F'. We prove $F \in \mathrm{SSAF}_\sigma(\alpha)$ by again considering two columns at a time; let $1 \leq \ell < r \leq n$.

1. If $\alpha_\ell \geq \alpha_r$ and $\beta_\ell \geq \beta_r$, then $\alpha_r \leq \beta_\ell$. We only need to confirm that type A triples containing a 1-cell within columns ℓ and r in F are inversion. If column ℓ contains the 1-entry in the basement, then $\beta_\ell = 0$, so $\alpha_r = 0$, and there are no type A triples to check. Otherwise, since $\alpha_r \leq \beta_\ell$, the 1-cells in column ℓ occur at a height greater than α_r and thus are not in a type A triple within these columns. Further, all type A triples with a 1-cell in column r contain two cells in column ℓ with entries greater than 1, so these triples are inversion.

2. If $\alpha_\ell < \alpha_r$ and $\beta_\ell < \beta_r$, then $\alpha_\ell < \beta_r$. We only need to confirm that type B triples containing a 1-cell within columns ℓ and r in F are inversion. Since $\alpha_\ell < \beta_r$, any 1-cells in column r occur at a height greater than $\alpha_\ell + 1$ and thus are not in a type B triple within these columns. Further, all type B triples with a 1-cell in column ℓ contain two cells in column r which have entries greater than 1, so these triples are inversion.

3. If $\alpha_\ell \geq \alpha_r$ and $\beta_\ell < \beta_r$, then $\alpha_r = \beta_r$ and $\sigma(\ell) < \sigma(r)$. Note that F contains no 1-cells in column r since $\sigma(r) > 1$ and $\alpha_r = \beta_r$. Since $\sigma(\ell) < \sigma(r)$, by case 2a of Lemma 2.8,

we have $F(\ell, i) < F(r, i+1)$ for all $0 \leq i \leq \beta_\ell$, yielding type A inversion triples $\{(\ell, i+1), (r, i+1), (\ell, i)\}$. The remaining type A triples in F contain two adjacent 1-cells in column ℓ and are inversion since column r contains no 1-cells.

4. If $\alpha_\ell < \alpha_r$ and $\beta_\ell \geq \beta_r$, then $\alpha_\ell = \beta_\ell$ and $\sigma(\ell) > \sigma(r)$. Note that F contains no 1-cells in column ℓ since $\sigma(\ell) > 1$ and $\alpha_\ell = \beta_\ell$. Since $\sigma(\ell) > \sigma(r)$, by case 1b of Lemma 2.8, we have $F(\ell, i) > F(r, i)$ for all $0 \leq i \leq \beta_r$, yielding type B inversion triples $\{(r, i+1), (\ell, i), (r, i)\}$. The remaining type B triples contain two adjacent 1-cells in column r and are inversion since column ℓ contains no 1-cells.

To finish the proof, note that the sum of the monomials $\mathbf{x}^{F'}$ over all $F' \in \mathrm{SSAF}_\sigma(\beta)$, where the only 1-entry is in the basement, is $\mathcal{A}^\sigma_\beta(0, x_2, \ldots, x_n)$. The factor $x_1^{|\alpha|-|\beta|}$ accounts for appending $|\alpha| - |\beta|$ cells with entry 1 to each of these fillings. □

Using the σ-extendable relation, we can define a covering relation $\lessdot_\sigma$ on weak compositions.

Definition 2.10. Set $\sigma_0 := \sigma$ and, for $0 \leq i \leq n-1$, let

$$\sigma_{i+1} = (\sigma_i(1) - 1, \ldots, \sigma_i(s_i - 1) - 1, \sigma_i(s_i + 1) - 1, \ldots, \sigma_i(n) - 1),$$

where $s_i = \sigma_i^{-1}(1)$. In words, σ_{i+1} is the permutation constructed from σ_i by deleting the element 1 and subtracting 1 from the remaining elements. We define the covering relation $\lessdot_\sigma$ so that $\beta \lessdot_\sigma \alpha$ if $\mathrm{len}(\beta) = \mathrm{len}(\alpha) - 1 = \ell$ and the weak composition $(\beta_1, \ldots, \beta_{s_k - 1}, 0, \beta_{s_k}, \ldots, \beta_\ell)$ is σ_k-extendable to α, where $k = n - \mathrm{len}(\alpha)$ (we must also have that $n \geq \mathrm{len}(\alpha)$).

By taking the transitive reflexive closure of $\lessdot_\sigma$, we can form weak compositions into a poset graded by length, since we lose one column each time we delete 1 from the basement. The polynomials $\mathcal{A}^\sigma_\alpha(\mathbf{x})$ are then given by sums over all saturated chains in this poset.

Theorem 2.11. *Atoms expand into summations over saturated chains, given by*

$$\mathcal{A}^\sigma_\alpha(\mathbf{x}) = \sum_{\beta_{(n)} \lessdot_\sigma \cdots \lessdot_\sigma \beta_{(1)} \lessdot_\sigma \alpha} x_1^{|\alpha|-|\beta_{(1)}|} x_2^{|\beta_{(2)}|-|\beta_{(1)}|} \cdots x_n^{|\beta_{(n)}|-|\beta_{(n-1)}|}.$$

Proof. Consider the expansion from Lemma 2.9:

$$\mathcal{A}^\sigma_\alpha(\mathbf{x}) = \sum_{\beta \ \sigma\text{-extendable to } \alpha} x_1^{|\alpha|-|\beta|} \mathcal{A}^\sigma_\beta(0, x_2, \ldots, x_n).$$

If $\beta_{s_0} > 0$, then β does not contribute to this sum, so assume $\beta_{s_0} = 0$ for each β summed over. Each $\beta_{(1)} \lessdot_\sigma \alpha$ is obtained by deleting the part β_{s_0} from such a β, so we may sum over $\beta_{(1)} \lessdot \alpha$. Then we have that $\mathcal{A}^\sigma_\beta(0, x_2, \ldots, x_n) = \mathcal{A}^{\sigma_1}_{\beta_{(1)}}(x_2, \ldots, x_n)$ where σ_1 is obtained by deleting 1 from σ and subtracting 1 from its remaining elements. Noting that $|\beta_{(1)}| = |\beta|$, we have a branching formula:

$$\mathcal{A}^\sigma_\alpha(\mathbf{x}) = \sum_{\beta_{(1)} \lessdot_\sigma \alpha} x_1^{|\alpha|-|\beta_{(1)}|} \mathcal{A}^{\sigma_1}_{\beta_{(1)}}(x_2, \ldots, x_n).$$

Recursively expanding our branching formula, we have

$$\begin{aligned}\mathcal{A}^\sigma_\alpha(\mathbf{x}) &= \sum_{\beta_{(n)} \lessdot_{\sigma_{n-1}} \cdots \lessdot_{\sigma_1} \beta_{(1)} \lessdot_\sigma \alpha} x_1^{|\alpha|-|\beta_{(1)}|} x_2^{|\beta_{(2)}|-|\beta_{(1)}|} \cdots x_n^{|\beta_{(n)}|-|\beta_{(n-1)}|} \\ &= \sum_{\beta_{(n)} \lessdot_\sigma \cdots \lessdot_\sigma \beta_{(1)} \lessdot_\sigma \alpha} x_1^{|\alpha|-|\beta_{(1)}|} x_2^{|\beta_{(2)}|-|\beta_{(1)}|} \cdots x_n^{|\beta_{(n)}|-|\beta_{(n-1)}|}.\end{aligned}$$

The final equivalence is possible by our definitions, which ensure that if $0 \leq k \leq n - \mathrm{len}(\alpha)$, then $\beta \lessdot_{\sigma_k} \alpha$ if and only if $\beta \lessdot_\sigma \alpha$. $\square$

Chapter 3

Previous Vertex Models

In this chapter, we detail relevant vertex models and results that we build on. Section 3.1 sketches Zinn-Justin's framework, which we extend to prove our results in Chapter 5. Section 3.2 shows Borodin and Wheeler's model when $q = t = 0$ along with the bijection of these fillings to SSAFs when $\sigma = \mathrm{id}$. Section 3.3 explains how the vertices in Brubaker, Buciumas, Bump and Gustafsson's model are essentially the same as in the models we consider, with some conventions changed.

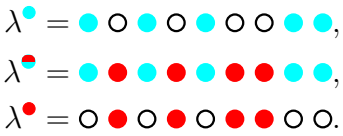
3.1 Zinn-Justin's framework for the product of Schur polynomials

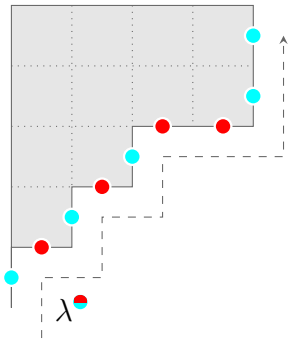
In this section, we sketch the derivation of Zinn-Justin's vertex model rule for Littlewood–Richardson coefficients $c^{\nu}_{\lambda\mu}$ [50]. Note again that Zinn-Justin proved a more general rule for the product of double Schur polynomials $s_\lambda(\mathbf{x}|\mathbf{y})$, but we have set $\mathbf{y} = \mathbf{0}$ to yield the case for Schur polynomials $s_\lambda(\mathbf{x})$. See Section 6.2 for discussion of double Schur polynomials.

3.1.1 The Schur model

We use coloured dots as labels instead of symbols; blue is a lighter shade than red. First, we re-encode the partition λ with a string of coloured dots in three ways. Enclose the Young diagram of λ in the upper-left corner of a rectangle with a North-East lattice path. Then we label North steps blue or white and label East steps red or white. Let $\lambda^{\color{cyan}\bullet}$ be the blue-white paths, $\lambda^{\color{blue}\bullet\color{red}\bullet}$ be the blue-red paths, and $\lambda^{\color{red}\bullet}$ be the white-red paths.

Example 3.1. Let $\lambda = (4, 4, 2, 1, 0)$. From the diagram below, we have





The model for Schur polynomials uses the following rhombic tiles with weights depicted below:

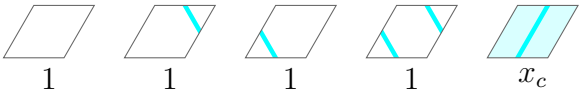
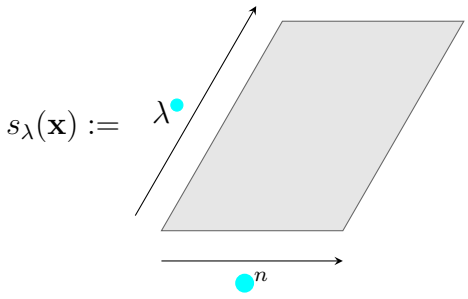
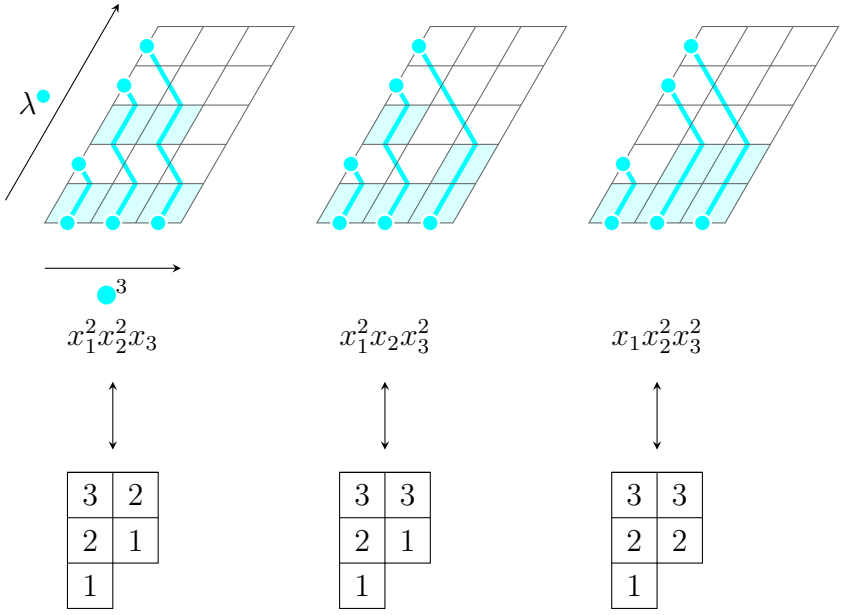


Figure 3.2: Tiles for the Schur model.

The tiles are placed within a rhombic lattice with n columns, numbered 1 to n from left to right. The final tile has weight x_c, where c is the column number that the tile occurs in, and all other tiles have weight 1. The left boundary of the model encodes λ with the string $\lambda^{\bullet}$, and the bottom boundary is a string of n blue dots, denoted $\bullet^n$. We call this model the ***Schur model***.:



Example 3.3. We compute $s_\lambda(\mathbf{x})$ for $\lambda = (2,2,1)$, so that $\lambda^- =$ ○ ● ○ ● ●. We have $s_\lambda(x_1,x_2,x_3) = x_1^2x_2^2x_3 + x_1^2x_2x_3^2 + x_1x_2^2x_3^2$.



We also show the "reverse" SSYTs associated with each tiling. For the bijection, follow the line starting in column i and record the column number c of each nontrivial tile it passes through in the i-th row of the Young tableau from left to right (rows are numbered 1 to n from bottom to top in the tableau). Instead of increasing, these tableaux will have entries that weakly decrease across rows and strictly decrease down columns. This effectively reverses the alphabet, but $s_\lambda(\tilde{\mathbf{x}}) = s_\lambda(\mathbf{x})$ since Schur polynomials are symmetric.

3.1.2 Vertex models for $c_{\lambda\mu}^\nu$

The proof involves gluing together three types of models tiled with rhombic tiles, in one of three orientations:

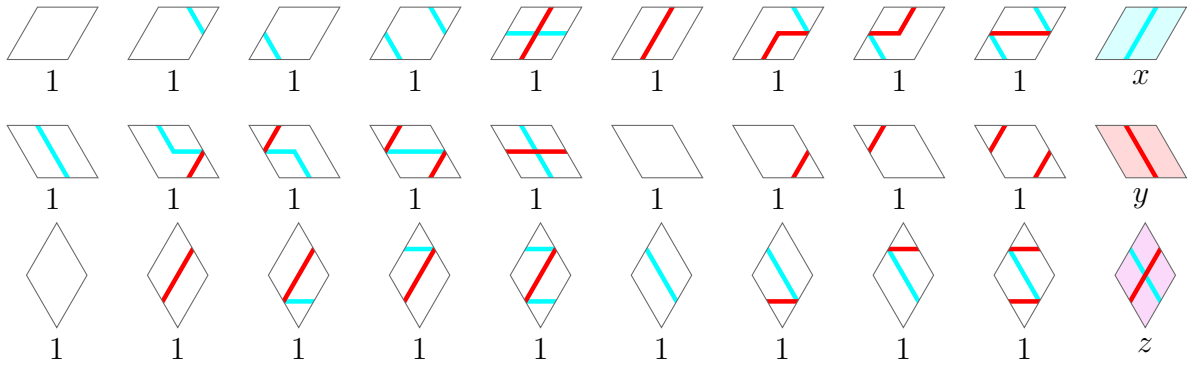
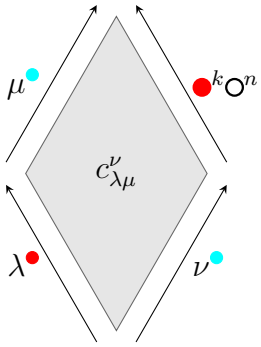


Figure 3.4: All tiles from [50].

The tiles with weight 1 are called ***trivial*** and the other tiles ***nontrivial***. The nontrivial tile in the third row is used for the expansion of two double Schur polynomials. For Schur polynomials, we set $x = x_c$, $y = -x_c$ and $z = 0$, so the final tile is not used. This tile is called the "equivariant" tile, called so because the expansion of the product of two double Schur polynomials corresponds to the equivariant cohomology of the Grassmannian.

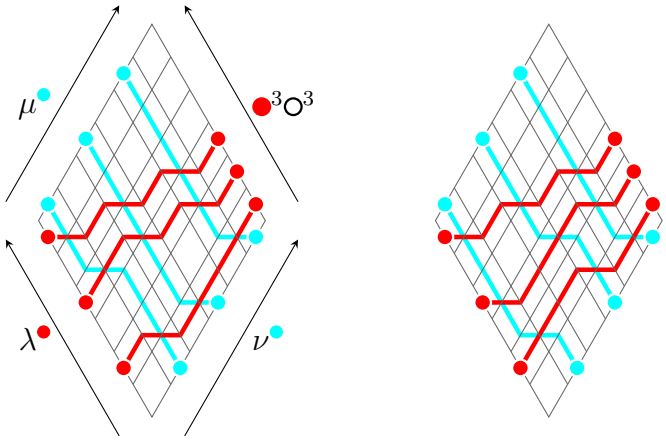
The structure coefficients $c^{\nu}_{\lambda\mu}$ are then calculated via a partition function using tiles from the third row of Figure 3.4, again where $z = 0$.

Theorem 3.5 ([50]). *The structure coefficients $c^{\nu}_{\lambda\mu}$ are computed by the partition function of the following model:*

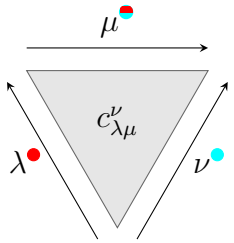


where $k = \max(\lambda)$ and $\bullet^k\circ^n$ is a sequence of k red dots followed by n white dots.

Example 3.6. When $\lambda = \mu = (2, 1, 0)$ and $\nu = (3, 2, 1)$, we have two fillings of the above model, showing $c^{\nu}_{\lambda\mu} = 2$:



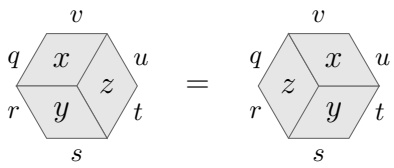
Remark 3.7. The top half of this picture will be fixed, so we can discard this half and tile the bottom with triangular tiles obtained by cutting the diamond tiles in half. This produces the triangular puzzles as in the right-hand image of Figure 1.2. The top boundary would then be $\mu^{\bullet}$:



3.1.3 The Yang–Baxter equation

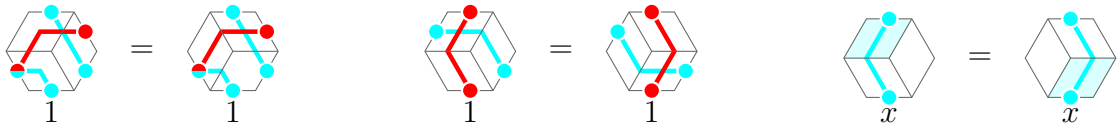
The key to the proof is the following Yang–Baxter equation.

Lemma 3.8 ([50]). *Let $x+y+z=0$. Fix the boundary of a unit hexagon as displayed, where dots $q,r,s,t,u,v \in \{\circ, \bullet, \bullet, \bullet\}$. We have the following equivalence of partition functions:*

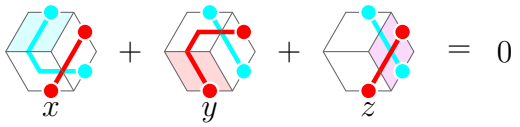


where the nontrivial weighted tiles have weight x, y and z as indicated.

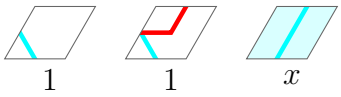
Example 3.9. In most cases, there is exactly one tiling of the hexagon on both sides of the equation, both having the same weight:



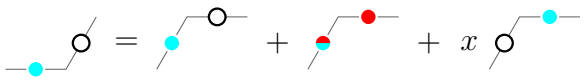
In the following case with boundary $(q, r, s, t, u, v) = (\circ, \circ, \bullet, \bullet, \bullet, \bullet)$, there is no way to tile the right-hand side of the equation, so it has weight 0. The left-hand side has weight $x + y + z$, which is why this sum is set to 0:



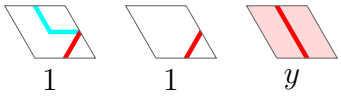
One might wonder how Lemma 3.8 is a Yang–Baxter equation. To understand this, let V be a vector space consisting of formal summations of edges (different angles are distinguished) labelled with a dot in $\{\circ, \bullet, \bullet, \bullet\}$. Then $\mathbf{R}(x)$ is a map from $V \otimes V$ to $V \otimes V$. We think of simple tensors as two edges glued together and imagine $\mathbf{R}(x)$ as mapping the bottom edges of a tile to top edges. For instance, note that we have three tiles in the first orientation with a blue dot on the bottom and a white dot on the right:



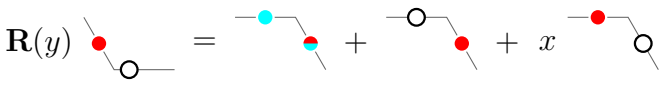
Then we have that $R(x)$ applied to these two bottom edges gives the following linear combination:



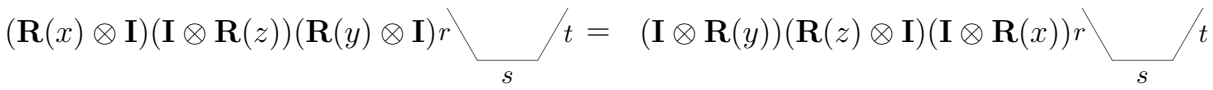
Similarly, there are three tiles in the second orientation with a white dot on the left and a red dot on the bottom:



This tells us:

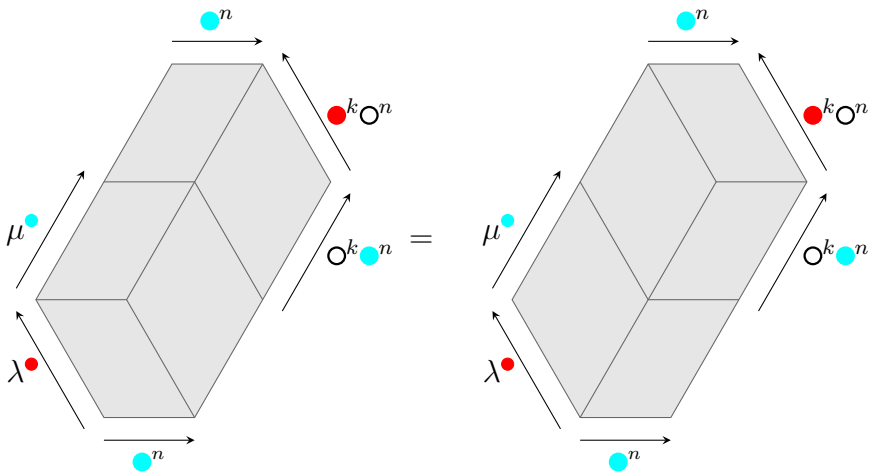


The tiles thus tell us how to define $\mathbf{R}(x)$ for single pairs of edges, and then we linearly extend this to summations of pairs of edges. The identity $\mathbf{I}$ does nothing to edges and then Lemma 3.8 manifestly is the Yang–Baxter equation applied to the three bottom edges of a unit hexagon labelled with $r, s, t \in \{$○, ●, ●, ◒$\}$:

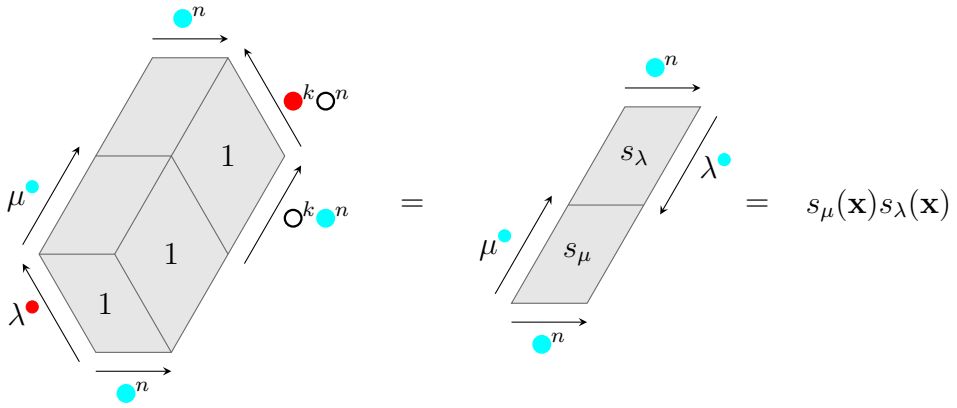


3.1.4 Sketch of proof

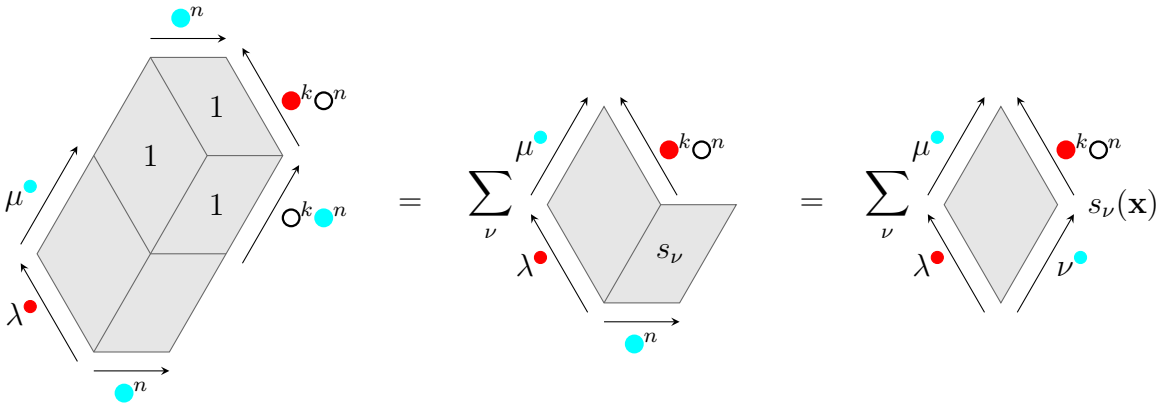
Sketch of proof of Theorem 3.5. We make a similar argument for our case in more detail in Section 5.2. The proof follows from repeatedly applying Lemma 3.8 to show the following equality of partition functions:



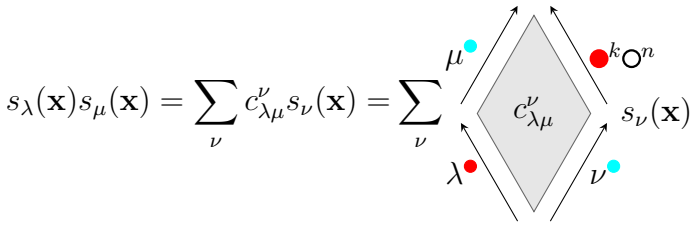
Next, we may delete certain fixed regions (which must have weight 1). We have the left-hand side is manifestly the product $s_\lambda(\mathbf{x})s_\mu(\mathbf{x})$:



On the right-hand side, we have:



This shows that the structure coefficients $c^{\nu}_{\lambda\mu}$ are computed by the diamond tiles since they determine the coefficients in the expansion of $s_\lambda(\mathbf{x})s_\mu(\mathbf{x})$:



□

3.2 Borodin and Wheeler's model for $E^{\sigma}_{\alpha}(\mathbf{x}; q, t)$

We give a simplified version of Borodin and Wheeler's [8] vertex model for nonsymmetric Macdonald polynomials [8] when $q = t = 0$ and $\sigma = \mathrm{id}$; in our conventions, this will compute $\mathcal{A}_{\tilde{\alpha}}(\tilde{\mathbf{x}})$.

Let $k = \max(\alpha)$ and $n = \mathrm{len}(\alpha)$. The model is constructed from a square grid with $k+1$ columns and n rows. Label the left of each row with 1 to n from bottom to top, label the right of each row with 0 and label the bottom of each column with the zero vector $\mathbf{0}$. The top boundary encodes α; we label the top of column $c \in \{0, \ldots, k\}$ with the binary vector $\boldsymbol{\alpha}(c) \in \{0,1\}^n$. The entry at index i in $\boldsymbol{\alpha}(c)$ is 1 if $\alpha_i = c$ and 0 otherwise.

$\mathcal{A}_{\tilde{\alpha}}(\tilde{\mathbf{x}}) =$

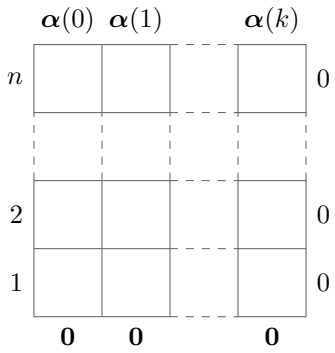


Figure 3.10: Schematic of Borodin and Wheeler's Vertex model for $\mathcal{A}_{\tilde{\alpha}}(\tilde{\mathbf{x}})$.

The model's vertices may be thought of as square tiles placed within this grid. The top and bottom sides of a tile are labelled by binary vectors in $\{0,1\}^n$. The left and right sides are labelled by single integers in $\{0, \ldots, n\}$. For $i \in [n]$, let the $\mathbf{e}_i$ denote the i-th standard basis vector. Given a vector $\mathbf{I} = (I_1, \ldots, I_n) \in \{0,1\}^n$ and $1 \leq a < b \leq n$, define $\mathbf{I}_{[a,b]} = \sum_{i=a}^{b} I_i$. The tiles and their corresponding weights are as given below:

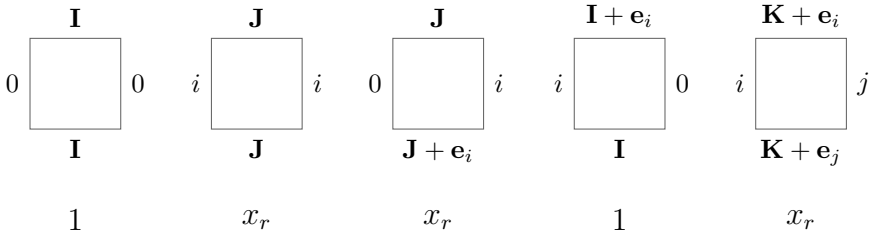
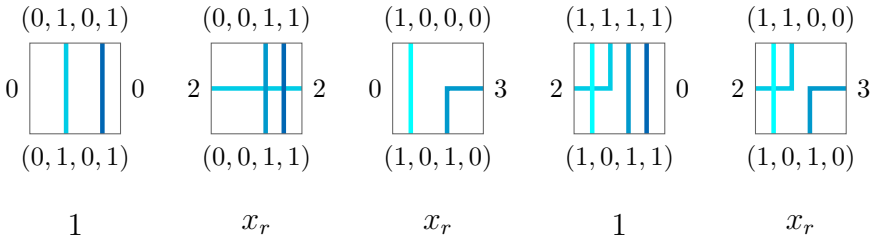


Figure 3.11: Tiles and weights for Borodin and Wheeler's models when $q = t = 0$. Here, $1 \leq i < j \leq n$, $\mathbf{J}_{[i,n]} = 0$ and $\mathbf{K}_{[j,n]} + \mathbf{K}_i = 0$. The index r in x_r is the row number the tile is placed in.

It is more intuitive to think of the tiles with decorations. We decorate tiles with coloured lines numbered with an integer in $[n]$. We draw lines moving vertically in their own "lanes" ordered 1 to n from left to right. One line may move horizontally across a tile, though it may turn upwards, and another line coming from below may take its place. Drawn this way, the rule is that a line i cannot move horizontally over a line j if $i < j$. Each tile is given the weight x_r if its right label is a positive integer, i.e. if a line exits on the right; otherwise, the tile has weight 1.

Example 3.12. We give examples of all five cases in Figure 3.11 with our conventions for decorating tiles.



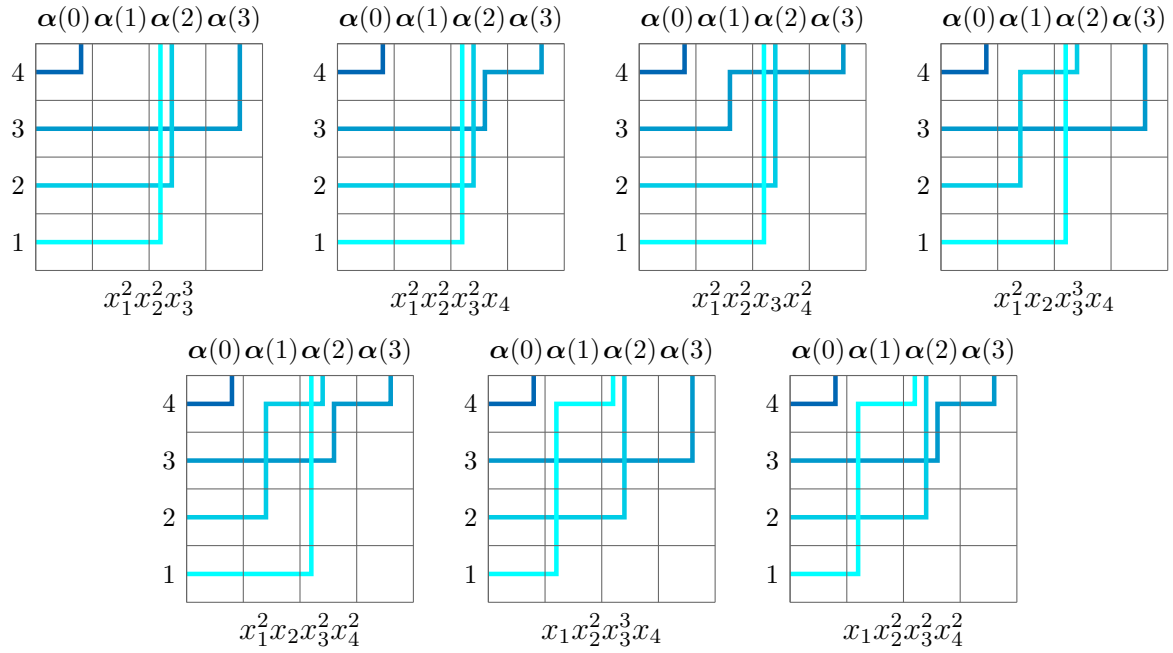
Note 3.13. In Borodin and Wheeler's model, the vectors $\mathbf{I}$ are in $\mathbb{N}^n$ to allow the lines to "wrap around" the lattice arbitrarily. When $q = 0$, this wrapping cannot occur. Accounting for the fact that there is also only one line of each colour in the model allows us to only consider *binary* vectors in the definition of the tiles, as we have done above.

The model in Figure 3.10 is tiled in all possible ways. We compute the partition function for one example.

Example 3.14. Let $\alpha = (2, 2, 3, 0)$. Then we have

$$\boldsymbol{\alpha}(0) = (0, 0, 0, 1), \quad , \boldsymbol{\alpha}(1) = (0, 0, 0, 0), \quad \boldsymbol{\alpha}(2) = (1, 1, 0, 0), \quad \boldsymbol{\alpha}(3) = (0, 0, 1, 0).$$

We display the seven tilings of the model with the weight of each tiling below:



From these tilings, we compute the partition function of the model:

$$\mathcal{A}_{\tilde{\alpha}}(\tilde{\mathbf{x}}) = x_1^2x_2^2x_3^3 + x_1^2x_2^2x_3^2x_4 + x_1^2x_2^2x_3x_4^2 + x_1^2x_2x_3^3x_4 + x_1^2x_2x_3^2x_4^2 + x_1x_2^2x_3^3x_4 + x_1x_2^2x_3^2x_4^2.$$

These fillings are in bijection with "reverse" SSAFs by our conventions. In these fillings, entries are weakly decreasing moving down columns. Further, for $\ell < r$, type A triples are now within columns where $\alpha_\ell \leq \alpha_r$ (instead of $\alpha_\ell \geq \alpha_r$) and type B triples are within columns where $\alpha_\ell > \alpha_r$ (instead of $\alpha_\ell < \alpha_r$). To obtain the associated SSAF, one can follow the line i from the left and, each time it moves horizontally within row r and crosses into a new column, record the entry r in the "reverse" SSAF (from bottom to top). We can convert this to an SSAF in our conventions by mapping each entry to e to $n - e + 1$ and then reversing the order of columns, shown in Figure 3.15.

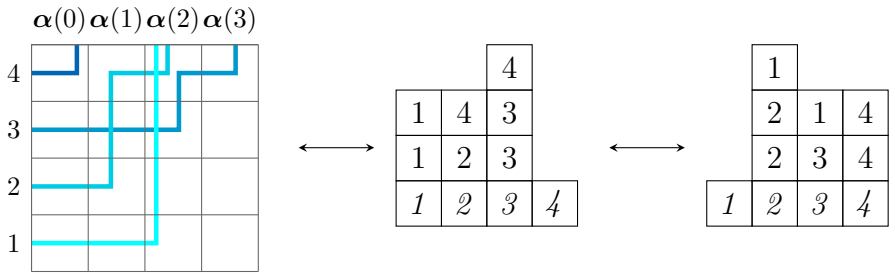


Figure 3.15: On the left, we have a tilling of Borodin and Wheeler's model for $\alpha = (2, 2, 3, 0)$. The middle is its associated "reverse" SSAF, and the right is the associated SSAF in our conventions.

3.3 BBBG model for Demazure atoms

In this section, we present the vertices of Brubaker, Buciumas, Bump and Gustafsson [9] for their vertex model for Demazure atoms. Below, we display their vertices and draw them in Zinn-Justin's style for the Schur model (after rotating by 90 degrees clockwise and reflecting across the vertical axis). These tiles are placed in a lattice similar to the Schur model, only with different boundary labels. We can think of these as coloured versions of the tiles of the Schur model:

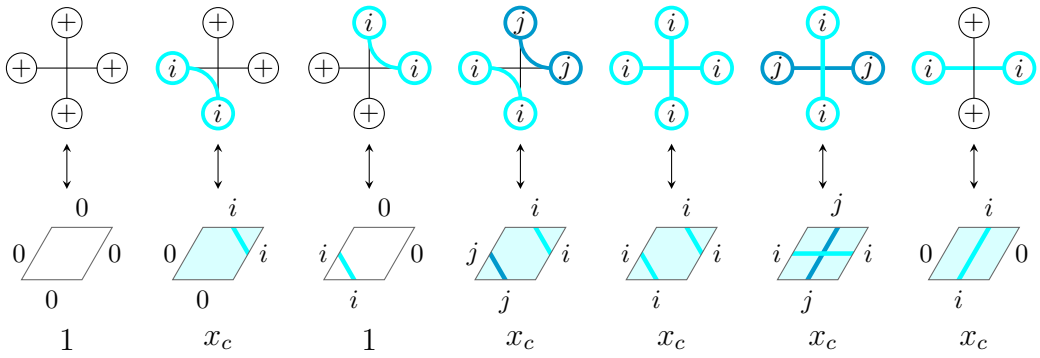


Figure 3.16: Brubaker, Buciumas, Bump and Gustafsson's vertices mapped to our drawing conventions. Here, $i, j \in [n]$ and $i < j$.

More tiles are nontrivial in this model, which picks up an extra factor $\mathbf{x}^\rho$; that is, the model computes $\mathbf{x}^\rho \mathcal{A}_\alpha(\mathbf{x})$. The model is essentially the same as ours in Section 4.1, except we remove these extra weights (only the final tile remains nontrivial) and have

different conventions for boundaries and colours. We could run this model through the same machinery of Section 5.2 (adjusting weights of other tiles introduced later), but we found that our conventions facilitate the proof when incorporating the permutation of the basement.

Chapter 4

Vertex Model Definitions

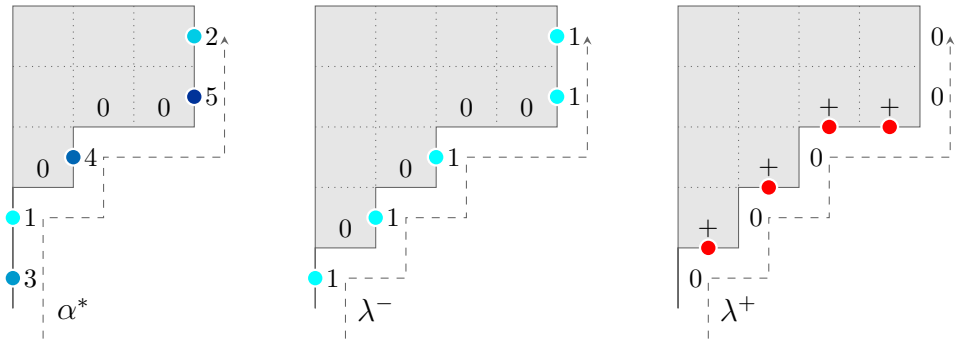
In this chapter, we define our model for the permuted-basement Demazure atoms $\mathcal{A}_\alpha^\sigma(\mathbf{x})$ and prove their correctness. Section 4.1 defines our model for atoms, which also yields the Schur polynomials of Section 3.1.1, aligning with the style of [48, 50]. Section 4.2 relates our model to a modified version of Borodin and Wheeler's. In Section 4.3, we show our model for atoms satisfies the branching formula in Theorem 2.11 and thus yields the same polynomials.

4.1 Vertex models for atoms and Schurs

In this section, we define our model for permuted-basement Demazure atoms $\mathcal{A}_\alpha^\sigma(\mathbf{x})$. Similar to Example 3.1, we label certain boundaries in our model with strings that re-encode α or λ. Let μ be the partition with the same parts as α. Enclose the Young diagram of μ within the top left corner of a rectangle with a North-East lattice path as depicted in Example 4.1. Label East steps 0. Each index $i \in [n]$ labels a North step in a row of width α_i; if multiple rows have the same width, their labels are sorted in descending order from bottom to top. We obtain the string α^* by reading labels along the lattice path, starting from the bottom.

We re-encode a partition λ similarly in two ways, with strings λ^- and λ^+, analogous to $\lambda^{\color{cyan}\bullet}$ and $\lambda^{\color{red}\bullet}$ from Section 3.1.1. For λ^-, label East steps 0 and North steps 1. For λ^+, label East steps with the symbol + and North steps 0. Read strings from the lattice path as before. The string λ^+ appears in later sections.

Example 4.1. Let $\alpha = (0, 3, 0, 1, 3)$ and $\lambda = (4, 4, 2, 1, 0)$. To produce α^*, we enclose the partition $\mu = (3, 3, 1, 0, 0)$. In this case, $\alpha_1 = \alpha_3 = 0$, so rows of width 0 are labelled 3 and 1 from bottom to top. Similarly, $\alpha_2 = \alpha_5 = 3$, so rows of width 3 are labelled 5 and 2 from bottom to top.



Reading the labels starting from the bottom produces the desired strings:

$$\alpha^* = 31040052,$$
$$\lambda^- = 101010011,$$
$$\lambda^+ = 0{+}0{+}0{+}{+}00.$$

Our models for atoms use the following rhombic tiles, depicted below, where $i, j, f, g \in [n]$, $i \leq j$ and $\sigma(f) < \sigma(g)$.

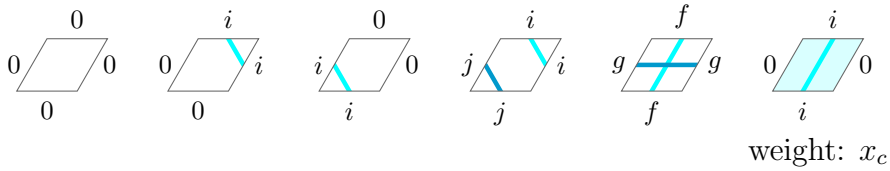
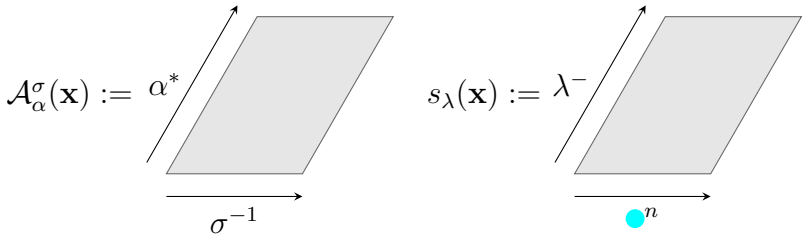


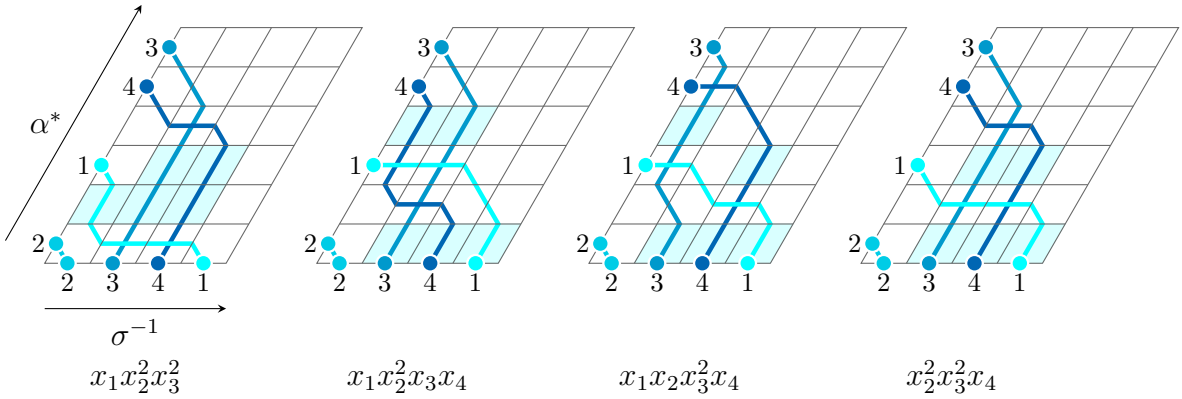
Figure 4.2: Tiles of the atom and Schur models.

The tiles are placed within a rhombic lattice with n columns, numbered 1 to n from left to right. The final tile has weight x_c, where c is the column number that the tile occurs in, and all other tiles have weight 1. Tiles of weight 1 are ***trivial*** and the final tile is ***nontrivial***. Labels between tiles and boundaries must match to be a legal tiling. We can also define the Schur polynomials exactly as in Section 3.1.1 using these tiles. We schematically outline both models below:



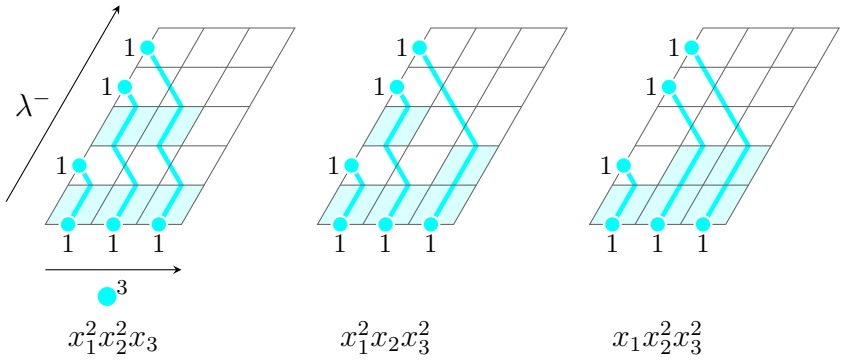
We call the model for $\mathcal{A}^{\sigma}_{\alpha}(\mathbf{x})$ the ***atom model*** and the model for $s_\lambda(\mathbf{x})$ the ***Schur model***. Label the left boundary of the atom model with α^* and the bottom with σ^{-1} (this choice makes our polynomials align with the definition in terms of skyline fillings in Section 2.2). Label the left boundary of the Schur model with λ^- and the bottom with all 1s, denoted $\bullet^n$. Label unspecified boundaries with 0s. The weight of a tiling is the product of its tile weights and the sum of all possible tilings is the partition function of the model.

Example 4.3. Let $\alpha = (1, 0, 2, 2)$ and $\sigma = (4, 1, 2, 3)$, so that $\sigma^{-1} = (2, 3, 4, 1)$ and $\alpha^* = 201043$. There are four tilings of the atom model, showing $\mathcal{A}^{\sigma}_{\alpha}(x_1, x_2, x_3, x_4) = x_1x_2^2x_3^2 + x_1x_2^2x_3x_4 + x_1x_2x_3^2x_4 + x_2^2x_3^2x_4$.



Also note that, with just one colour, say 1, we can define the Schur polynomials as they are defined in Example 3.1, only labelling blue dots with 1. We redo Example 3.3.

Example 4.4. Next, let $\lambda = (2, 2, 1)$, so that $\lambda^- = 01011$. There are three tilings of the Schur model, showing $s_\lambda(x_1, x_2, x_3) = x_1^2x_2^2x_3 + x_1^2x_2x_3^2 + x_1x_2^2x_3^2$.



4.2 Relating to previous vertex models

Borodin and Wheeler [8] had the idea of permuting the colours on the left side of the model we present in Section 3.2 to account for permuted basements:

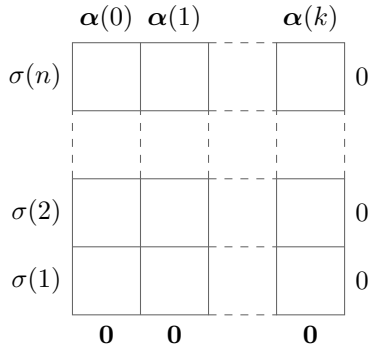


Figure 4.5: Schematic of Borodin and Wheeler's model with permutation σ on the left boundary.

As we have seen in Section 3.2, our conventions differ slightly from theirs so that their models compute $\mathcal{A}_{\tilde{\alpha}}^{\sigma^{-1}}(\tilde{\mathbf{x}})$. We switched conventions to make their model compute $\mathcal{A}_{\alpha}^{\sigma}(\mathbf{x})$ by the definition in Section 2.2. Then we modified the tiles so that lines are not "fused" to make them compatible with the Zinn-Justin framework. As stated in Section 3.3, these tiles are also essentially the same as Brubaker, Buciumas, Bump and Gustafsson [9], now depending on a permutation. Below is a tiling of the modified version of the Borodin and Wheeler model (rotated 90 degrees counter-clockwise) with the corresponding tiling in our model. The similarity is clear:

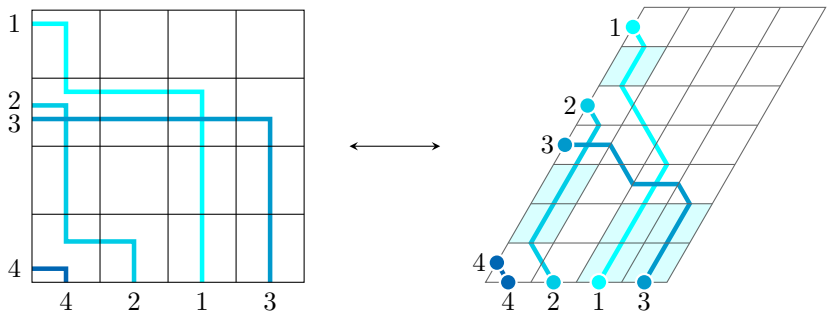


Figure 4.6: Modified version of Borodin and Wheeler's model and a corresponding tiling for our model in the case that $\alpha = (3, 2, 0, 2)$ and $\sigma = (3, 2, 4, 1)$; hence, $\sigma^{-1} = (4, 2, 1, 3)$ is encoded on the bottom.

Thus, we have combined Borodin and Wheeler's idea of permuting the colours to incorporate the basement, applied this to the BBBG model, and inserted it into Zinn-Justin's framework. A model with lines "fused" like in Borodin and Wheeler's might be possible to squeeze into this framework, but we found multiple arbitrary choices for defining "diamond" tiles like those in Section 5.1, making the search space for a Yang–Baxter equation large.

4.3 Equivalence of atom model and skyline definition

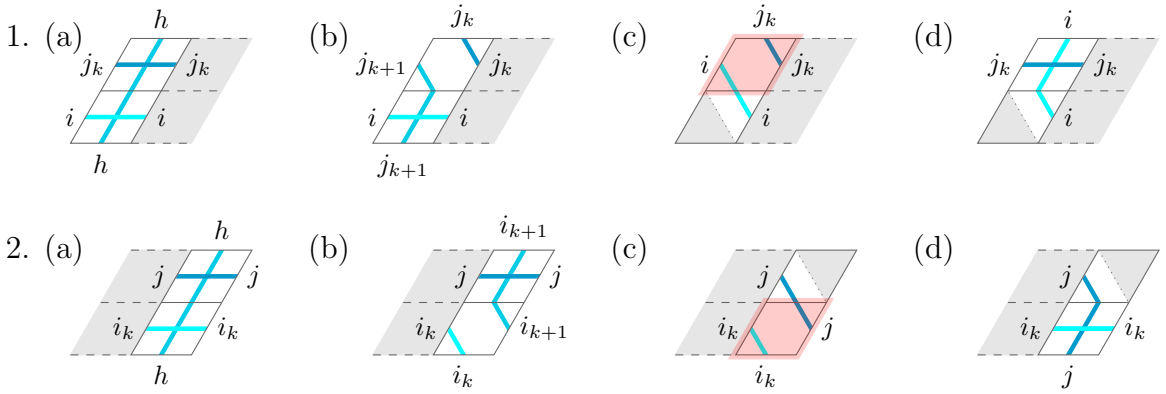
We show that the atom model satisfies Theorem 2.11 and thus yields the same polynomials. We call a string of nonnegative integers a ***descending string*** if it does not contain the consecutive substring ij for two positive integers $i < j$. In other words, a descending string can ascend after a 0, but not after a positive integer. Note that, by our encoding procedure, α^* is descending.

The key to our argument is that columns $2, \ldots, n$ also compute a permuted-basement Demazure atom on a different weak composition, say β, for precisely all β that are σ-extendable to α. However, we must first show that the vertical between columns encodes a weak composition in a similar way to β^*; to do this, we want to show that the vertical is always a descending string.

Lemma 4.7. *Within a tiling of the atom model, verticals between columns encode descending strings (moving up).*

Proof. Descending strings label the left and right boundaries. Assume that there is not a descending string between two columns, so there is a position in this vertical where colour i is directly below j and $i < j$. Set $i_0 := i$ and $j_0 := j$.

We consider tiling to the left in case 1 and tiling to the right in case 2, both situations having four subcases:



Case 1a transmits i and j_k to the left in the same order. In 1b, we must have $j_{k+1} > j_k > i$. A sequence of cases 1a and 1b then transmits some non-descending string containing ij_k for $i < j_k$ to the left, which cannot continue perpetually since the left boundary is descending. The highlighted tile in 1c is not possible since we maintain $i < j_k$. If 1d occurs after a case of 1b, then line i crosses the same line j_k twice, which is not possible. Thus, case 1d must occur, possibly after some cases of 1a, and line $i = i_0$ crosses line $j = j_0$.

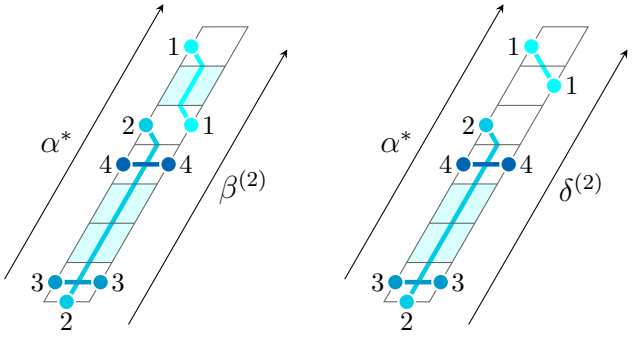
A similar argument forces lines i and j to cross moving to the right, but then i and j cross twice, which is not possible. Thus, intermediate verticals are also descending strings. □

We show that the first column in the atom model essentially sums over all $\beta_{(1)} \preccurlyeq_\sigma \alpha$, satisfying Theorem 2.11, thus yielding the same polynomials as in the skyline formulation. Note that Lemma 4.7 shows that we may assume the right side of the first column is descending. This side will encode a weak composition β where $\beta_s = 0$ with a string similar to β^*, only skipping over the character $s = \sigma^{-1}(1)$. We call this string $\beta^{(s)}$ and obtain it by deleting the character s from β^* and appending 0 to the end.

Example 4.8. Let $\alpha = (3, 2, 0, 2)$ and $\sigma = (4, 1, 2, 3)$, so that $\sigma^{-1} = (2, 3, 4, 1)$ and $s = \sigma^{-1}(1) = 2$. There are two ways to tile column 1 so that the right side is a descending

string. These strings encode weak compositions $\beta = (2, 0, 0, 2)$ and $\delta = (3, 0, 0, 2)$. We compute the boundary strings:

$$\alpha^* = 3004201 \qquad \beta^* = 3200410 \qquad \beta^{(2)} = 3004100$$
$$\delta^* = 3200401 \qquad \delta^{(2)} = 3004010$$



To make the first column's relationship with σ-extendability more explicit, we relate them to the hypotheses from Definition 2.7. The position a line i exits on the left determines α_i and the position i enters on the right determines β_i (where $\beta_i = 0$ if line i enters at the bottom of the column). Let $1 \leq \ell \leq r \leq n$. We have four cases:

1. If $\alpha_\ell \geq \alpha_r$ and $\beta_\ell \geq \beta_r$, then line ℓ always stays above line r, which entails $\alpha_r \leq \beta_\ell$.
2. If $\alpha_\ell < \alpha_r$ and $\beta_\ell < \beta_r$, then line ℓ always stays below line r, which entails $\alpha_\ell < \beta_r$.
3. If $\alpha_\ell \geq \alpha_r$ and $\beta_\ell < \beta_r$, then line r must cross horizontally over line ℓ, which entails $\alpha_r = \beta_r$ and $\sigma(\ell) < \sigma(r)$.
4. If $\alpha_\ell < \alpha_r$ and $\beta_\ell \geq \beta_r$, then line ℓ must cross horizontally over line r, which entails $\alpha_\ell = \beta_\ell$ and $\sigma(\ell) > \sigma(r)$.

Next, we prove this intuition more technically.

Lemma 4.9. *The first column in the atom model is possible to tile if and only if $\beta^{(s)}$ labels its right side, where $s = \sigma^{-1}(1)$ and β is σ-extendable to α.*

Proof. We have argued above that we may assume the right side of the first column always encodes a weak composition β, where $\beta_s = 0$, with the string $\beta^{(s)}$. We must show that it is possible to tile the model if and only if β is σ-extendable to α. Note that both strings β^* and $\beta^{(s)}$ will have β_i instances of the character 0 before the character i, determining the size of part i. Suppose it is possible to tile the first column and let $1 \leq \ell < r \leq n$.

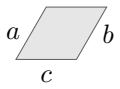
1. If $\alpha_\ell \geq \alpha_r$ and $\beta_\ell \geq \beta_r$, then the label r occurs below the label ℓ on the left side. If $\ell = s$, then $\beta_\ell = \beta_r = 0$ and line ℓ begins on the bottom side of the column and crosses line r. Then $\alpha_r = \beta_r = 0$ and thus $\alpha_r \leq \beta_\ell$. Otherwise, lines ℓ and r do not cross. Let $i \leq r$ be the smallest integer where $\alpha_i = \alpha_r$ and $j \geq \ell$ be the largest integer where $\beta_j = \beta_\ell$. If line i exits on the left at height h, then line j must exit on the right at height at least h, which implies $\alpha_r \leq \beta_\ell$.

2. If $\alpha_\ell < \alpha_r$ and $\beta_\ell < \beta_r$, then the label ℓ occurs below r on both sides of the column and the lines do not cross. Let $i \leq \ell$ be the smallest integer where $\alpha_i = \alpha_\ell$ and $j \geq r$ be the largest integer where $\beta_j = \beta_r$. If line i exits on the left at height h, then line j must enter on the right at a height $h' \geq h + 1$ and there must be a 0 between height h and h' on the right, which implies $\alpha_\ell < \beta_r$.

3. If $\alpha_\ell \geq \alpha_r$ and $\beta_\ell < \beta_r$, we have $r \neq s$ since $\beta_r > 0$; thus, line r must cross horizontally over line ℓ, so $\alpha_r = \beta_r$ and $\sigma(\ell) < \sigma(r)$.

4. If $\alpha_\ell < \alpha_r$ and $\beta_\ell \geq \beta_r$, suppose $\ell = s$; then $\beta_r = 0$. Line ℓ must cross vertically under all lines $i \geq \ell$ where $\alpha_i = 0$, so $\alpha_r \leq \alpha_\ell$, contradicting our assumptions. Otherwise, line ℓ must cross horizontally over line r, so $\alpha_\ell = \beta_\ell$ and $\sigma(\ell) > \sigma(r)$.

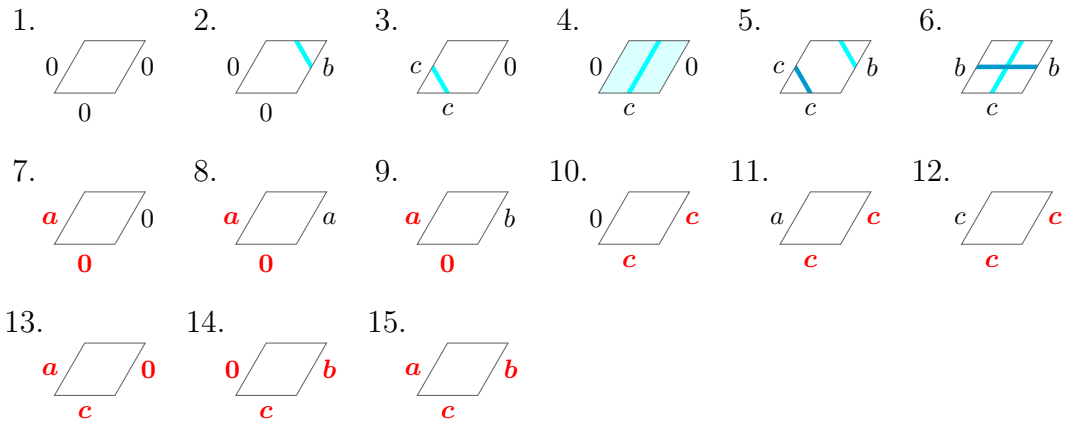
Conversely, suppose β is σ-extendable to α and $\beta_s = 0$. Label the left of column 1 with α^* and the right with $\beta^{(s)}$. We show that it is always possible to tile this column from the bottom up, considering one tile at a time. Let the left, right and bottom edges of the tile under consideration have labels a, b, c:



Let the current tile be at height h. Let $L(h)$ be the number of 0s below height h on the left side of the column and let $R(h)$ be the number of 0s below height h on the right side. If a and b are positive integers, we have $\alpha_a = L(h)$ and $\beta_b = R(h)$, respectively. We say the ***zero condition*** is satisfied at height h when

$$L(h) = \begin{cases} R(h) - 1 & \text{if } c = 0 \\ R(h) & \text{if } c > 0. \end{cases}$$

The zero condition is satisfied when $h = 1$, where $c = s > 0$ and $L(h) = R(h) = 0$. Let a, b and c be distinct positive integers. There are 15 cases for the tile at height h:



We have emphasized problematic clusters of labels in bold red font. We want to show that only cases 1-6 are possible and a tile may always be placed in these cases; this will also ensure we satisfy the zero condition at height $h+1$, so by induction, we can tile the entire column.

1-4. It is always possible to place a tile in these cases.

5. We must show that $b < c$ to have a valid tile; suppose $c < b$. Then line b exits on the left at a height above h and, since α^* is a descending string, we must have $\alpha_c < \alpha_b$. We must also have that $\beta_c \leq \beta_b$; if $c = s$ and $\beta_c = \beta_b$, we have that $\sigma(c) > \sigma(b)$ by case 4 of Definition 2.7, which is not possible since $\sigma(c) = 1$. Otherwise, $c = s$ and $\beta_c < \beta_b$ or $c \neq s$, and we still have $\beta_c < \beta_b$ since $\beta^{(s)}$ is a descending string. By case 2 of Definition 2.7, we have that $\alpha_c < \beta_b$, but $\alpha_c = L(h) = R(h) = \beta_b$; hence, $b < c$.

6. For the crossing to occur, we must show $\sigma(c) < \sigma(b)$. If $c = s$, then $\sigma(c) = 1 < \sigma(b)$, as desired. Othewise, if $c < b$, then $\alpha_c \geq \alpha_b$ and $\beta_c < \beta_b$, so $\sigma(c) < \sigma(b)$ by case 3 of Definition 2.7. If $b < c$, then $\alpha_b < \alpha_c$ and $\beta_b \geq \beta_c$, so $\sigma(b) > \sigma(c)$ by case 4 of Definition 2.7.

7-9. These cases cannot occur since then line a enters on the right at height at least h; since $L(h) < R(h)$, we have $\alpha_a < \beta_a$.

10-12. These cases cannot occur since then line c enters the column on the bottom or right twice, which is not possible.

13. Since we assume $\alpha_a = L(h) = R(h)$ and the right label is 0, this case implies $\alpha_a < \beta_a$, which is not possible.

14. We have that α_b and α_c are greater than both β_b and β_c because of the 0 on the left. Thus, we cannot satisfy Definition 2.7 since each case implies $\alpha_d \leq \beta_e$ for at least one pair $d, e \in \{b, c\}$.

15. This case implies line a must enter on the right side at a height above h. This is only possible if $\beta_a = \beta_b$ and $a < b$, otherwise $\alpha_a < \beta_a$. On the left side, labels b and c must be above a, so we have $\alpha_b \geq \alpha_a$ and $\alpha_c \geq \alpha_a$.

    We cannot have that $\alpha_b = \alpha_a$ since $a < b$, so $\alpha_a < \alpha_b$. If $\alpha_c = \alpha_a$, then $c < a < b$ and $\alpha_c < \alpha_b$; note that $\beta_c \leq \beta_b$. If $\beta_c < \beta_b$, then by case 2 of Definition 2.7, we have $\alpha_c < \beta_b$, meaning c must have exited at a previous step. If $\alpha_c = \alpha_b$, we are in case 4 of Definition 2.7 and $\sigma(c) > \sigma(b)$, meaning it is not possible that $c = s$; otherwise, $\alpha_c = \beta_c$, meaning $\beta_c = \beta_b$, which is not possible since $\beta^{(s)}$ is a descending string.

    Thus, $\alpha_b > \alpha_a$ and $\alpha_c > \alpha_a$, implying that α_b and α_c are both greater than β_b and β_c, and we cannot satisfy Definition 2.7 for the same reason as in case 14.

□

We now justify that the atom model yields the same polynomials as those given in Section 2.2.

Theorem 4.10. *The polynomials given by the atom model satisfy the branching formula in Theorem 2.11.*

Proof. By Lemma 4.9, we can consider a sum over β that are σ-extendable to α, where $\beta_s = 0$, so we may instead sum over all $\beta_{(1)} \lessdot_\sigma \alpha$, where $\beta_{(1)} = (\beta_1, \ldots, \beta_{s-1}, \beta_{s+1}, \ldots, \beta_n)$. For each $\beta_{(1)}$, the first column will have weight $x_1^{|\alpha|-|\beta_{(1)}|}$.

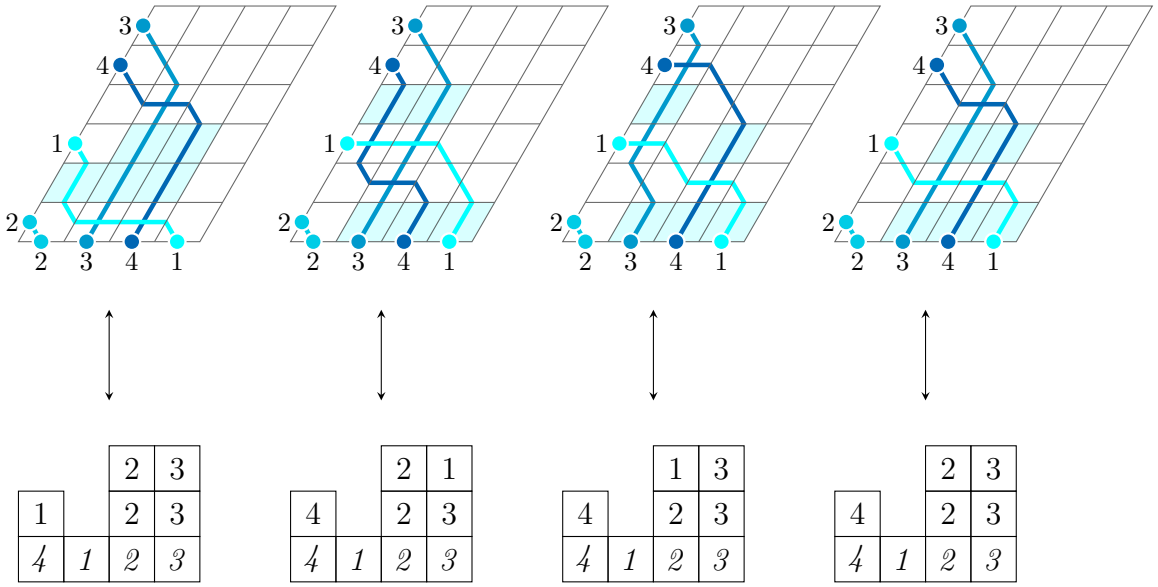
Considering the columns $2, \ldots, n$ separately, with $\beta^{(s)}$ along the left boundary, we set each colour $i > s$ equal to $i - 1$. The left boundary will then be $\beta^*_{(1)}$ and the bottom boundary will be σ_1^{-1}, where σ_1 is as in Definition 2.10. If we let σ_1 determine the crossing tiles instead of σ, this is the model for $\mathcal{A}^{\sigma_1}_{\beta_{(1)}}(x_2, \ldots, x_n)$. The tilings of this model are identical to the columns $2, \ldots, n$ in the original picture, only with the colours $i > s$ decreased by 1. Thus, we have the same branching formula as in Theorem 2.11 and can expand the polynomials as before:

$$\begin{aligned}\mathcal{A}^{\sigma}_{\alpha}(\mathbf{x}) &= \sum_{\beta_{(1)} \lessdot_\sigma \alpha} x_1^{|\alpha|-|\beta_{(1)}|} \mathcal{A}^{\sigma_1}_{\beta_{(1)}}(x_2, \ldots, x_n) \\ &= \sum_{\beta_{(n)} \lessdot_\sigma \cdots \lessdot_\sigma \beta_{(1)} \lessdot_\sigma \alpha} x_1^{|\alpha|-|\beta_{(1)}|} x_2^{|\beta_{(2)}|-|\beta_{(1)}|} \cdots x_n^{|\beta_{(n)}|-|\beta_{(n-1)}|}.\end{aligned}$$

□

Similar to [8] and Section 3.2, we may obtain the SSAF corresponding to a tiling by simply following line i to produce the entries in column i. Begin with a skyline diagram of shape α with basement σ and other entries blank. For each line labelled i in a tiling, follow line i from the bottom, moving up. Each time line i moves through a nontrivial tile within a column c, assign the entry c to the bottom-most blank entry of column i in the skyline diagram.

Example 4.11. We show the corresponding SSAFs for the tilings in Example 4.3, where $\alpha = (1, 0, 2, 2)$ and $\sigma = (4, 1, 2, 3)$, so $\sigma^{-1} = (2, 3, 4, 1)$ and $\alpha^* = 201043$. *Note that columns in SSAFs are numbered* 1 *to* n *from left to right. Columns are not numbered by their basement entries.*



Chapter 5

Vertex Models for $a^{\beta}_{\alpha\lambda}(\sigma)$

In this chapter, we present our vertex models for the structure coefficients $a^{\beta}_{\alpha\lambda}(\sigma)$. In Section 5.1, we present the tiles for our model and state our main result, Theorem 5.3. The majority of the proof is completed in Section 5.2, but we reserve proof of the key Yang–Baxter equation, referred to as the Column Lemma 5.8, for Section 5.3.

5.1 Theorem statement

Our models use the "diamond" tiles below where $f, g, h, i \in [n]$, $\sigma(f) < \sigma(g)$ and $\sigma(f) < \sigma(h)$. The label b^+ indicates that a blue line b shares that edge with a red line. The label ab indicates that blue lines a and b, with $\sigma(a) < \sigma(b)$, share that edge. All tiles have weight 1.

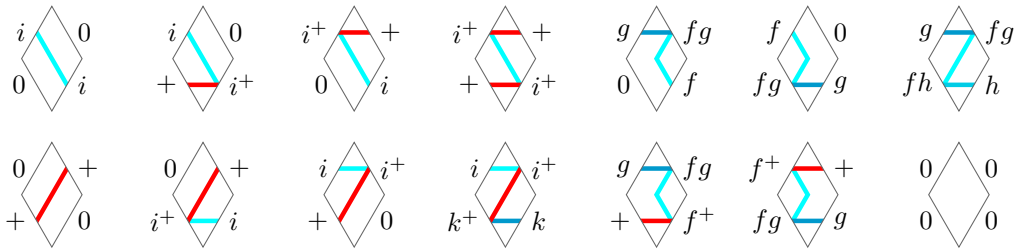


Figure 5.1: Tiles of the model for $a^{\beta}_{\alpha\lambda}(\sigma)$.

In addition to having labels match, we must also ban certain adjacencies not captured

by the labels, as depicted in Figure 5.2. We do not allow a line of colour i to move diagonally directly below a line of colour j if $i < j$. These restrictions are still local and can be imposed with additional labels (see Appendix A), but we exclude them to avoid clutter.

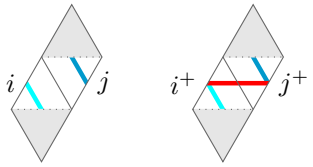
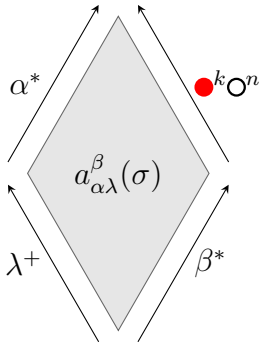


Figure 5.2: Banned adjacencies, where $1 \leq i < j \leq n$.

Theorem 5.3. *The structure coefficients $a^{\beta}_{\alpha\lambda}(\sigma)$ are calculated as the partition function of the model*

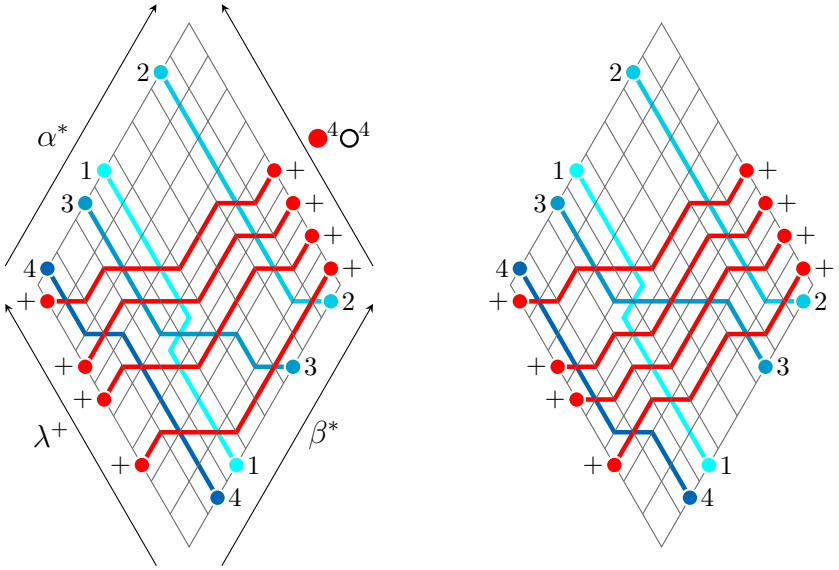


where $k = \max(\beta)$ and the restrictions in Figure 5.2 apply within. The symbol $\bullet^k\circ^n$ represents the string $+^k0^n$.

Proof. We reserve this proof for Section 5.2. □

We call our vertex model for $a^{\beta}_{\alpha\lambda}(\sigma)$ the ***atom–Schur model***. Recall that we assume α, β and λ have length n, but we may append zeros to match their lengths. Similarly, we may append zeros to the end of the string α^* and append $+$ symbols to the end of λ^+ so that these strings all have length $n + k$.

Example 5.4. For $\alpha = (1,3,1,0)$, $\lambda = (3,1,0,0)$ and $\beta = (1,4,3,1)$, we have $k = \max(\beta) = 4$. If $\sigma(1) < \sigma(3)$, there are two tilings, showing $a^{\beta}_{\alpha\lambda}(\sigma) = 2$, otherwise line 3 may not cross horizontally over line 1 and $a^{\beta}_{\alpha\lambda}(\sigma) = 0$.

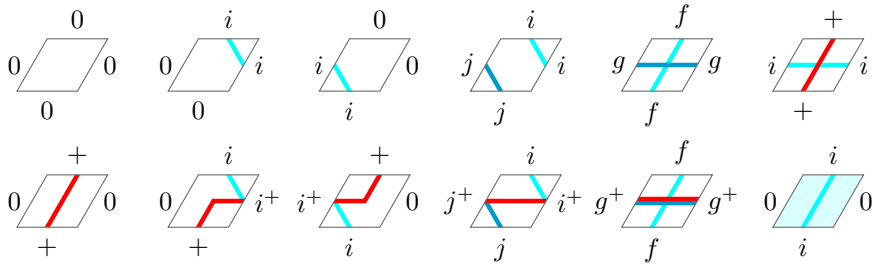


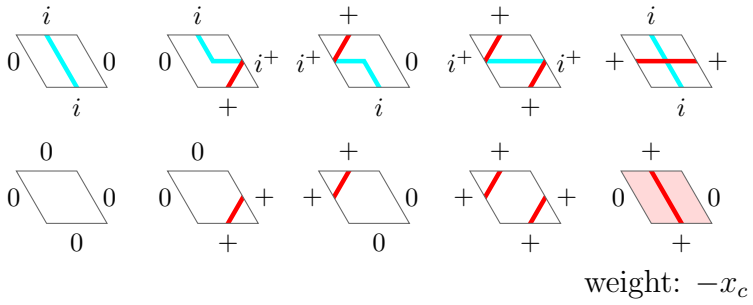
Remark 5.5. The atom–Schur model may be cut in half because the top half is always fixed, giving a triangular puzzle rule as in [48, 50]. The example in Figure 1.3 is obtained from Example 5.4 this way, where the top part of the triangle encodes α in a similar way to α^*, only with + in place of 0.

5.2 Proof of Theorem 5.3

We put the three models in one picture as in the framework of Example 3.1 to show Theorem 5.3. The crucial machinery for this proof is a restricted Yang–Baxter equation, which we refer to as the Column Lemma 5.8. New tiles are necessary, which expand the previous set and introduce a new orientation.

Figure 5.6 depicts the complete set of tiles. We call the first, second and third sets of tiles ***right-sheared***, ***left-sheared*** and ***diamond*** tiles, respectively. These may be thought of as the "coloured" analogues of Zinn-Justin's tiles depicted in Example 3.1, where crossings are allowed. The left-sheared tiles contain a new nontrivial tile of weight $-x_c$, which allows fillings of negative weight that may cancel with others. We again depict





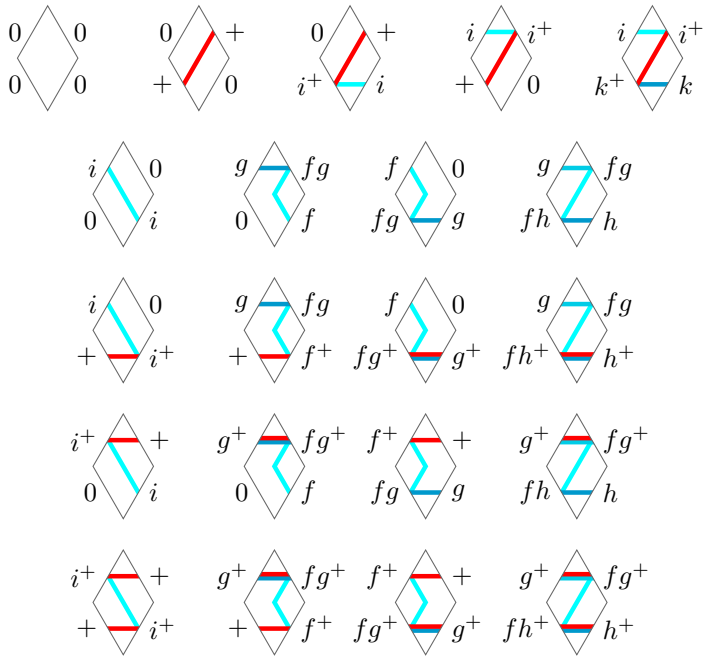
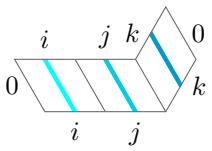


Figure 5.6: The full set of tiles where $f, g, h, i, j, k \in [n]$, $i \leq j$, $\sigma(f) < \sigma(g)$ and $\sigma(f) < \sigma(h)$.

vertex models with grey diagrams tiled only with tiles of matching orientation. Left- and right-sheared tiles share the same column number c if one is on top of the other; columns are numbered 1 to n from left to right. Some tiles now have "double" red and blue lines; these tiles facilitate the proof, but may be excluded in Theorem 5.3 as they will not occur when the boundaries are set as we have them.

We still ban adjacencies between diamond tiles as in Figure 5.2, but there are no restrictions between tiles that are not both diamonds. Left-sheared tiles are unaffected; for example, the following configuration is legal for *any* i, j and k in $[n]$:

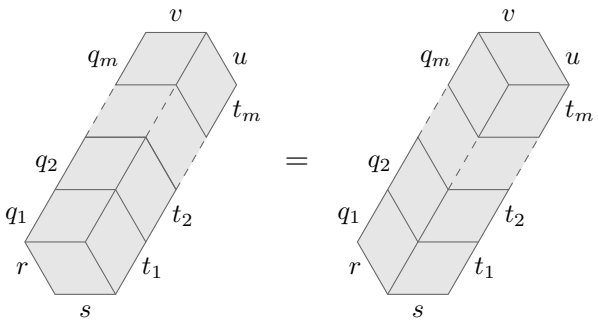


Remark 5.7. Diamond tiles are determined by cutting all trivial right-sheared tiles into triangles and gluing them together in all possible ways. This introduces new labels responsible for the restrictions in Figure 5.2. We suppress these extra labels to clean up the analysis, but show them in Appendix A. The left-sheared tiles are not determined this way and do not allow crossings between blue lines.

We found that these conditions allow the different models used in our framework to interact properly; for instance, the region labelled **A** in Figure 5.12 must allow left-sheared tiles to be unconcerned with the colours of their neighbouring tiles to travel up as desired. Further, our choices permit the Yang–Baxter equation in Lemma 5.8, which we state next.

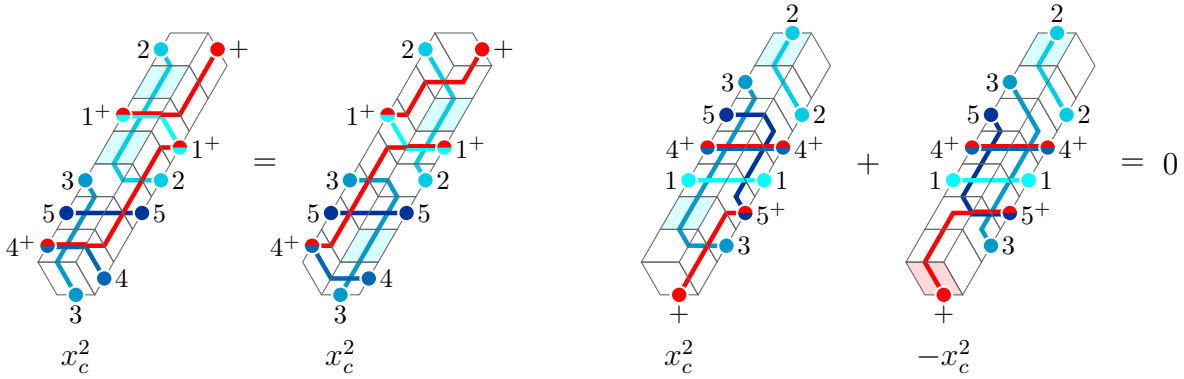
The key to our proof is a restricted Yang–Baxter equating columns of tiles. See Section 6.1 for contrast and discussion of our equation and Zinn-Justin's in Lemma 3.8. The tiles in Figure 5.6 are minimal in the sense that this lemma does not hold if we remove any tile.

Lemma 5.8 (The Column Lemma)**.** *Let $q_1, \ldots, q_m$, r, s, $t_1, \ldots, t_m$, u, v be fixed labels where $r, u \in \{0, +\}$. We have the following equality of partition functions:*

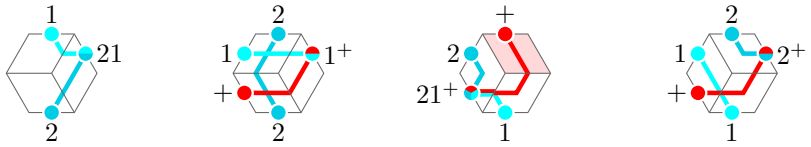


Proof. We reserve this proof for Section 5.3. □

Example 5.9. We consider two examples of Lemma 5.8, where σ is chosen appropriately to allow the given crossings. In the first example, both sides have weight x_c^2. In the second, there are two ways to tile the column on the left-hand side, which cancel, and so there is no way to tile the column on the right-hand side.

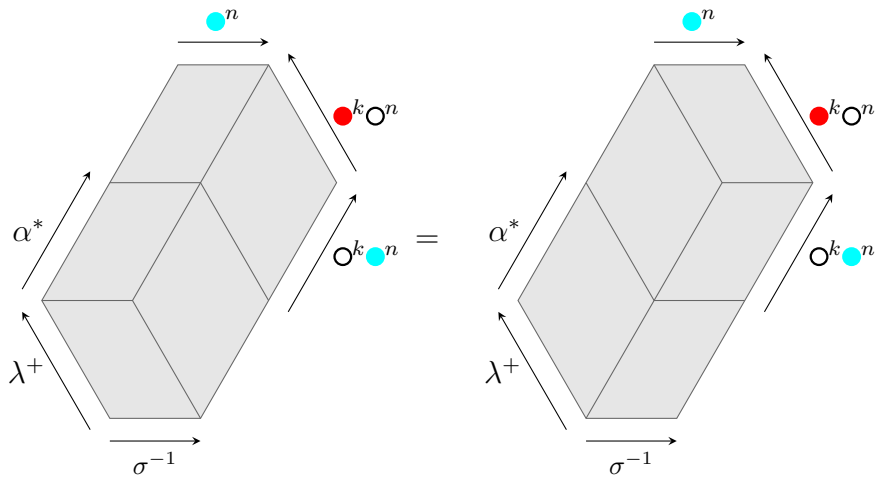


Example 5.10. The following unit hexagons are cases where r or u is not in $\{0, +\}$ and there is no way to complete the other side of the equation with our tiles. Here, we suppose $\sigma(2) < \sigma(1)$.

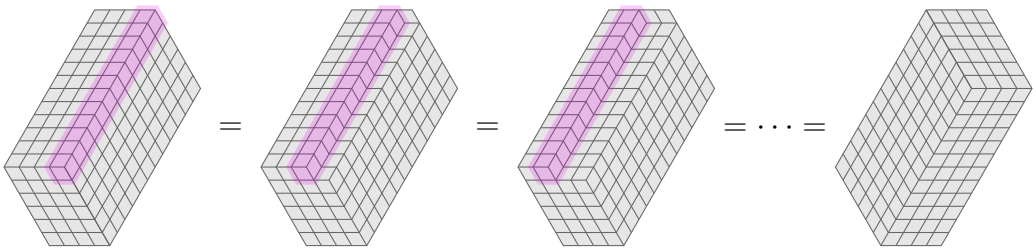


Interpreting the next lemma proves our result.

Lemma 5.11. *Set $k = \max(\alpha) + \max(\lambda)$. The following configurations have the same partition function:*



Proof. Repeatedly applying the Column Lemma 5.8 to internal columns of length $2(k+n)$, from right to left, top to bottom, shows equality. We illustrate this schematically, omitting the boundaries:



The boundary conditions ensure that the southwest and northeast labels of columns we equate are always in $\{0, +\}$ at every stage in this process, allowing repetition of Lemma 5.8. □

The proof now follows from examining both sides of the equation in Lemma 5.11. In short, the left-hand side is manifestly the product $\mathcal{A}^{\sigma}_{\alpha}(\mathbf{x})s_{\lambda}(\mathbf{x})$ and the right-hand side is manifestly the summation $\sum_{\beta} a^{\beta}_{\alpha\lambda}(\sigma)\mathcal{A}^{\sigma}_{\alpha}(\mathbf{x})$ where $a^{\beta}_{\alpha\lambda}(\sigma)$ is the partition function of the atom–Schur model.

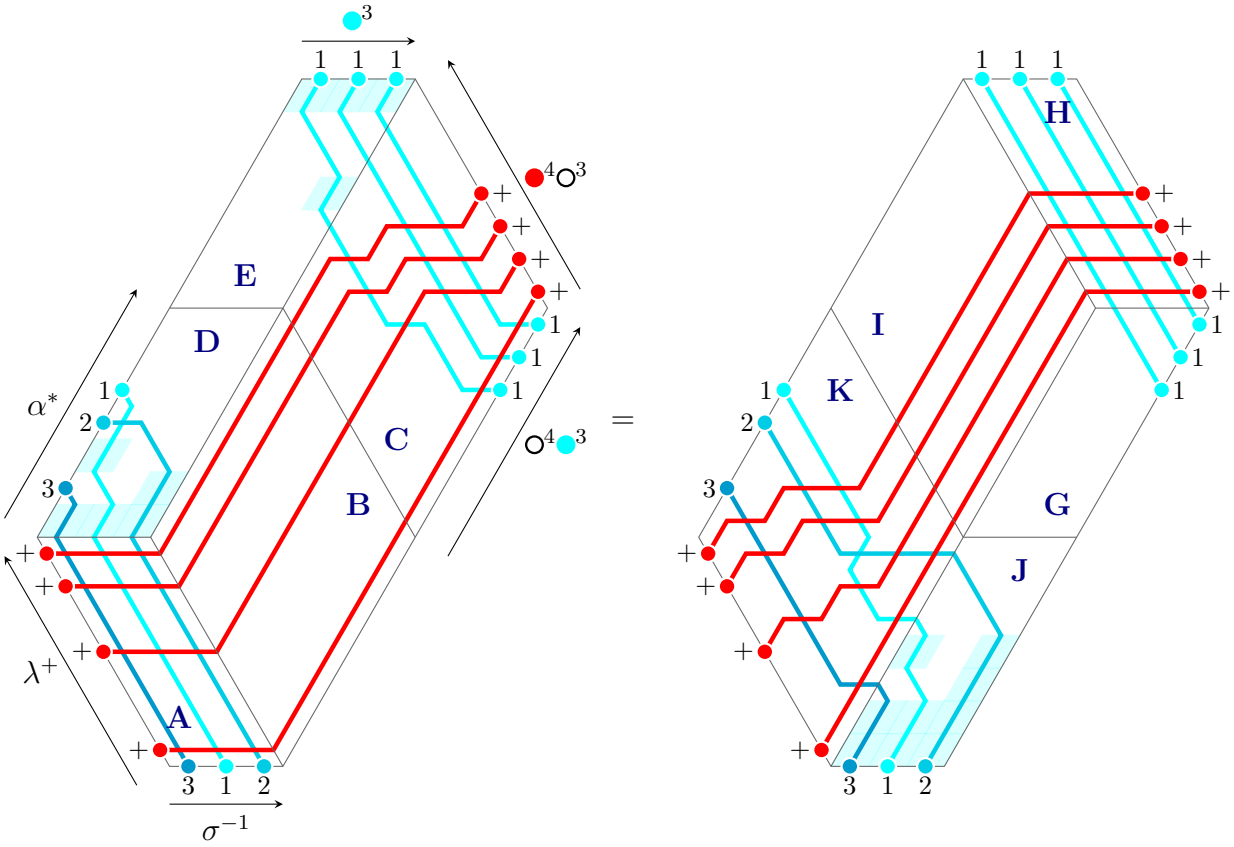


Figure 5.12: Two tilings of weight $x_1^3x_2^2x_3^4$ from the configurations in Lemma 5.11 where $\lambda = (2,2,1)$, $\sigma = (2,3,1)$ and $\alpha = (2,2,1)$, so that $n = 3$, $k = 4$ and $\sigma^{-1} = (3,1,2)$. Regions are labelled to facilitate exposition.

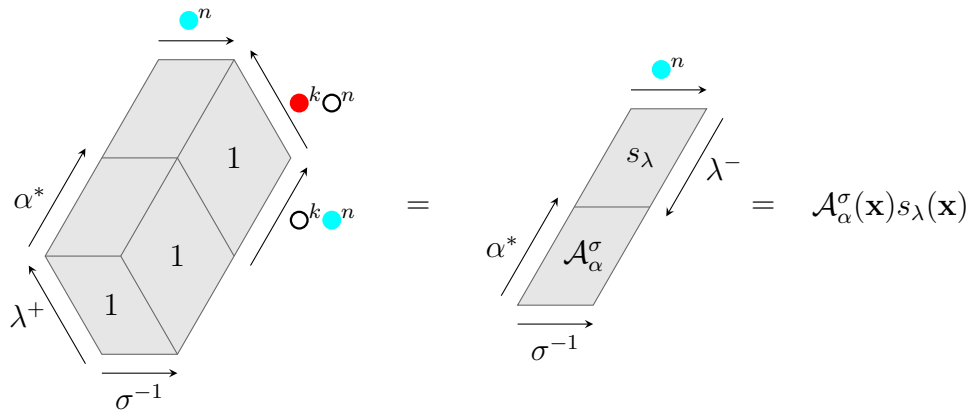
Note 5.13. Before proceeding with the proof, we note a few differences from our main theorem:

1. In this section, we have included extra diamond tiles with "double" red and blue lines; however, these tiles will only occur at intermediate steps when applying the Column Lemma 5.8 as in the proof of Lemma 5.11. They will not occur when filling the atom–Schur model, so we omit them in the statement of Theorem 5.3.

2. We have set $k = \max(\lambda) + \max(\alpha)$, but when considering only a particular case where β is given, it suffices to set $k = \max(\beta)$, as is done in Theorem 5.3.

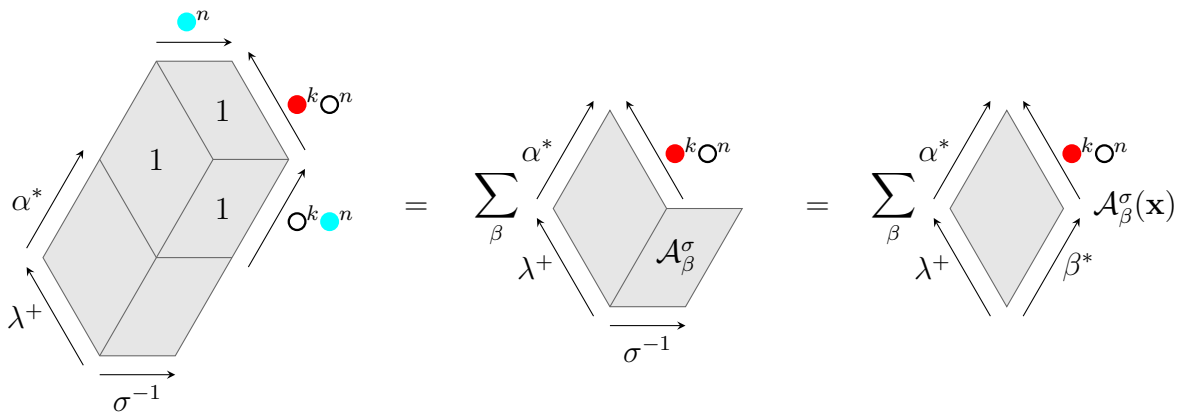
Proof of Theorem 5.3. See the illustration in Figure 5.12 where we label regions **A**, **B**, ..., **K**. Within region **A**, all blue lines must move northwest and all red lines must move east. The red lines continue straight northeast through **B**, transmitting the string λ^+ to the southwest boundary of **C**. Lemma 10 in [50] says that there is only one way to tile **C**, which forces the shared boundary between **C** and **E** to be the string λ^- upside-down. Thus, regions **A**, **B** and **C** have weight 1.

Next, we recognize region **D** as the atom model $\mathcal{A}^\sigma_\alpha(\mathbf{x})$. From the previous paragraph, we have that λ^- is upside-down on the southeast boundary of **E**. Rotating region **E** by 180 degrees, we see that it is the Schur model for $s_\lambda(\mathbf{x})$ with the variables in reverse order; since $s_\lambda(\mathbf{x})$ is symmetric, the weight of the left-hand side is the product $\mathcal{A}^\sigma_\alpha(\mathbf{x}) s_\lambda(\mathbf{x})$. We summarize pictorially:

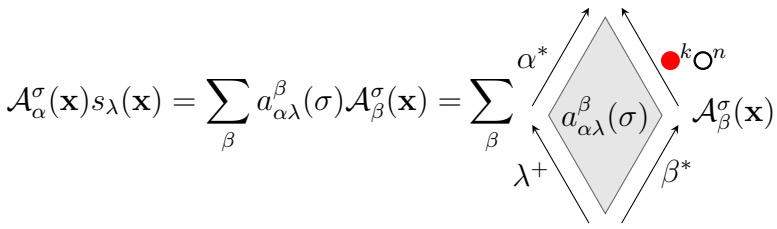


On the right-hand side, the regions **G**, **H** and **I** always have weight 1 and cross as in Figure 5.12. Within region **J**, all blue lines must exit the northwest boundary if they are to reach the northwest boundary of **K** (our choice of k makes the boundary long

enough to ensure this). The blue lines then travel through the boundary between **J** and **K**, varying over strings β^* that encode weak compositions β (these strings will be descending by a similar argument made in Lemma 4.7). For each β^* along this boundary, we recognize region **J** as $\mathcal{A}^{\sigma}_{\beta}(\mathbf{x})$ and region **K** as the atom–Schur model from Theorem 5.3. Thus, the right-hand side is a summation over compositions β where each summand is a product of the atom–Schur model $a^{\beta}_{\alpha\lambda}(\sigma)$ and $\mathcal{A}^{\sigma}_{\beta}(\mathbf{x})$. Again, summarizing pictorially:



By Lemma 5.11, we can equate both sides. This shows that the structure coefficients $a^{\beta}_{\alpha\lambda}(\sigma)$ are computed by the diamond tiles since they determine the coefficients in the expansion of $\mathcal{A}^{\sigma}_{\alpha}(\mathbf{x})s_{\lambda}(\mathbf{x})$:



□

5.3 Proof of the Column Lemma 5.8

We prove the key technical result of this thesis, the Column Lemma 5.8. We first show that the lemma holds when only trivial tiles are used in Lemma 5.15. Next, most cases

are handled by induction in Lemma 5.17. Finally, we complete the proof by handling the cases not amenable to induction.

For a label $q \in \{b, b^+\}$ with $b \in [n]$, we refer to its colour by $\#(q) = b$ and set $\#(0) = \#(+) = 0$. We may mark an edge labelled q with a symbol to indicate restrictions on q. The symbol ○ indicates $q = 0$, ⊕ indicates $\#(q) = 0$ and ⊛ indicates $\#(q) \in [n]$. We sometimes draw illustrations with colours of certain labels equal; doing this has the effect of uncrossing lines, altering the following tiles:

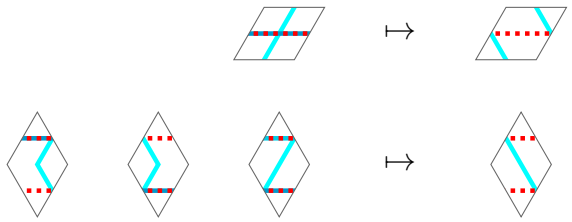
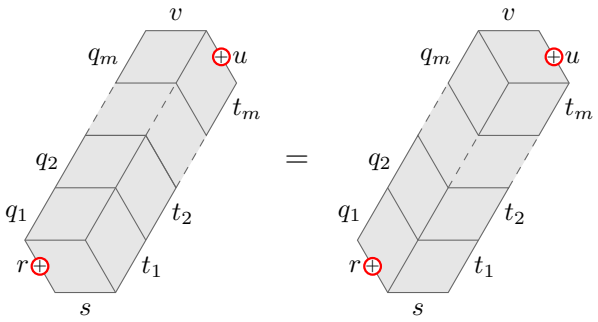


Figure 5.14: Uncrossing lines. Dotted red lines indicate a red line may be present or not.

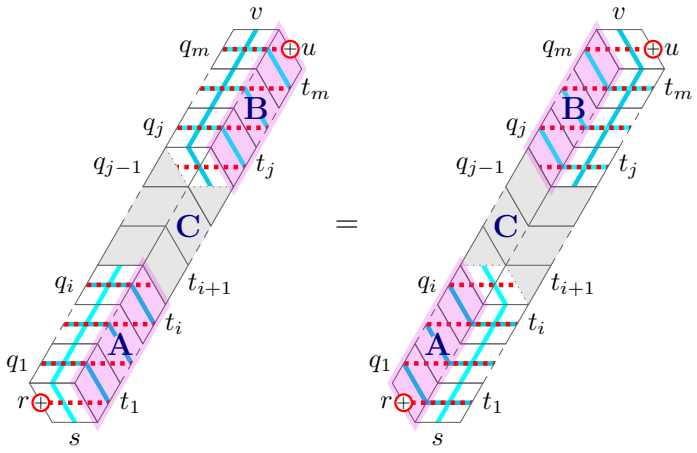
Restating Lemma 5.8 with our conventions, we wish to prove:



We first show that Lemma 5.8 is true when both columns use only trivial tiles, that is, when $x_c = 0$.

Lemma 5.15. *Lemma 5.8 is true when $x_c = 0$.*

Proof. As stated in Remark 5.7, diamond tiles are produced by taking trivial right-sheared tiles, cutting them into triangles, and gluing them together in all possible ways. Left-sheared tiles behave differently, not allowing crossings. The result is that columns with only trivial tiles are decorated identically unless $0 < s < \#(t_1)$ or $v > \#(q_m) > 0$. We outline the general case where both of these are true:



In the left column, line s crosses vertically under some contiguous sequence of lines that exit at $q_1, \ldots, q_i$. The index i is the smallest integer where $\#(t_{i+1}) \leq s < \#(q_i)$ or $i = m$. Within the right column, line s must turn to the left after exiting the tile labelled by t_i. A similar situation is forced in the top region for the line v. The grey regions **C** are identical in both columns. In the illustration, we have uncrossed lines exiting at $q_1, \ldots, q_i$ or $q_j, \ldots q_m$; if crossings are allowed, they will appear identical in regions both labelled **A** or **B**. □

We proceed by induction on m. In light of the following lemma, the base case $m = 1$ holds.

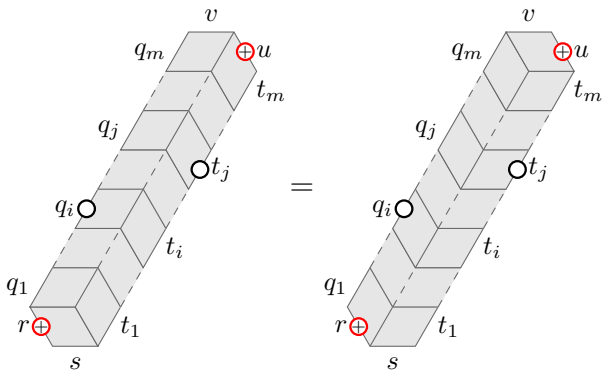
Lemma 5.16. *The unit hexagons with the following restrictions are equivalent:*



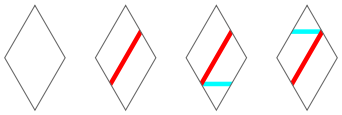
Proof. Both equations follow from brute force. Note that r and u are unrestricted in the second equation. □

Many cases are now possible to prove by induction.

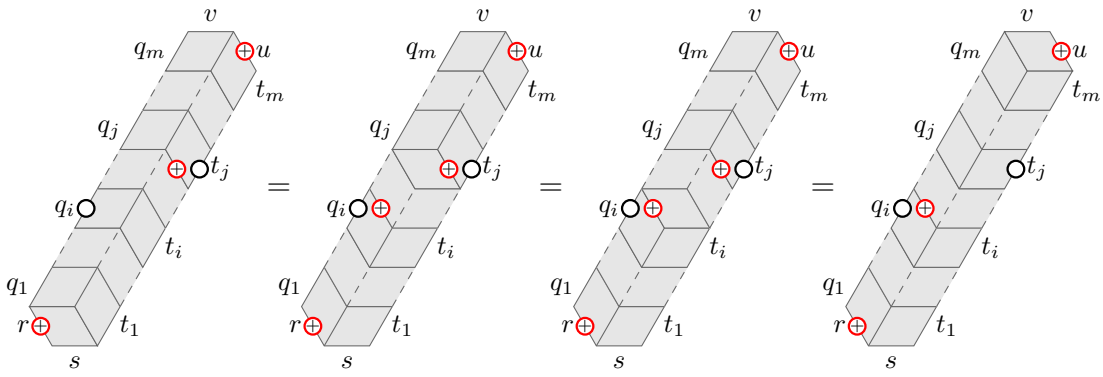
Lemma 5.17. *Assume that Lemma 5.8 holds for columns of length $m - 1 \geq 1$. Then if $q_i = t_j = 0$ for $1 \leq i \leq j \leq m$, we have:*



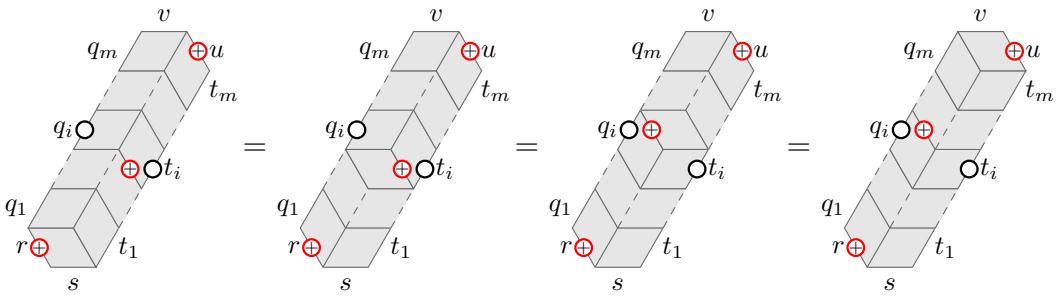
Proof. Note that if the northwest or southeast edge of a diamond tile is 0, then the northeast or southwest edge, respectively, must be in $\{0, +\}$ since these are the only such tiles:



From this fact, we know some internal edges are in $\{0, +\}$, which we label with the $\oplus$ symbol. If $i < j$, we have the following equivalences by applying Lemma 5.8 three times, going backwards part of the way in the second equality:



If $i = j$, we have the following equivalences, where the second equality follows from applying the second equation in Lemma 5.16:

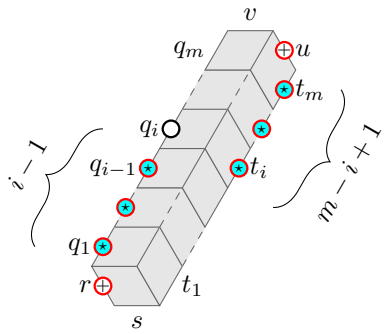


□

Since r and u are in $\{0, +\}$, there can be at most $m + 1$ separate blue lines within a column, entering at $s, t_1, \ldots, t_m$ and exiting at $v, q_1, \ldots, q_m$. The next lemma shows that we can assume at least $m - 1$ separate blue lines.

Lemma 5.18. *Lemma 5.8 holds for columns of length m containing less than $m - 1$ separate blue lines.*

Proof. If $q_i \neq 0$ for all $1 \leq i \leq m$, there are at least m separate blue lines within a column. Otherwise, let i be the smallest integer with $q_i = 0$, so there is a blue line at q_k for $1 \leq k < i$. By Lemma 5.17, we can assume that $t_j \neq 0$ for $i \leq j \leq m$. This accounts for $(i - 1) + (m - i + 1) = m$ edges incident with a blue line:

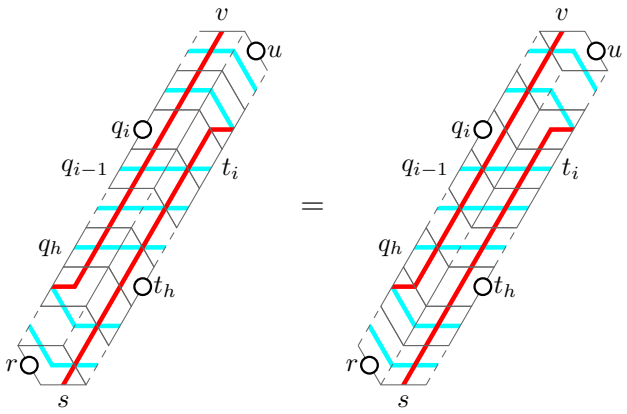


The line entering at t_i may exit at q_{i-1}, but none of the lines entering at $t_{i+1}, \ldots, t_m$ may exit at $q_1, \ldots, q_{i-1}$, accounting for at least $m - 1$ separate blue lines. □

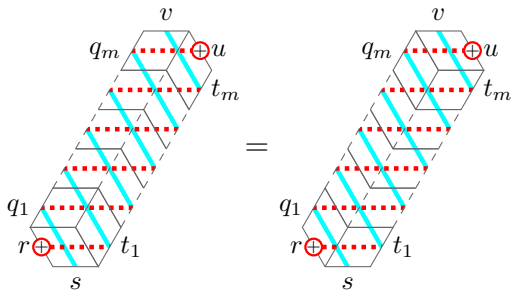
We now prove Lemma 5.8 by handling the remaining cases.

Proof of the Column Lemma 5.8. From Lemma 5.18, we only need to consider the cases of a column with at least $m-1$ separate blue lines. We again set labels equal, uncrossing blue lines, to show the general structure of tilings.

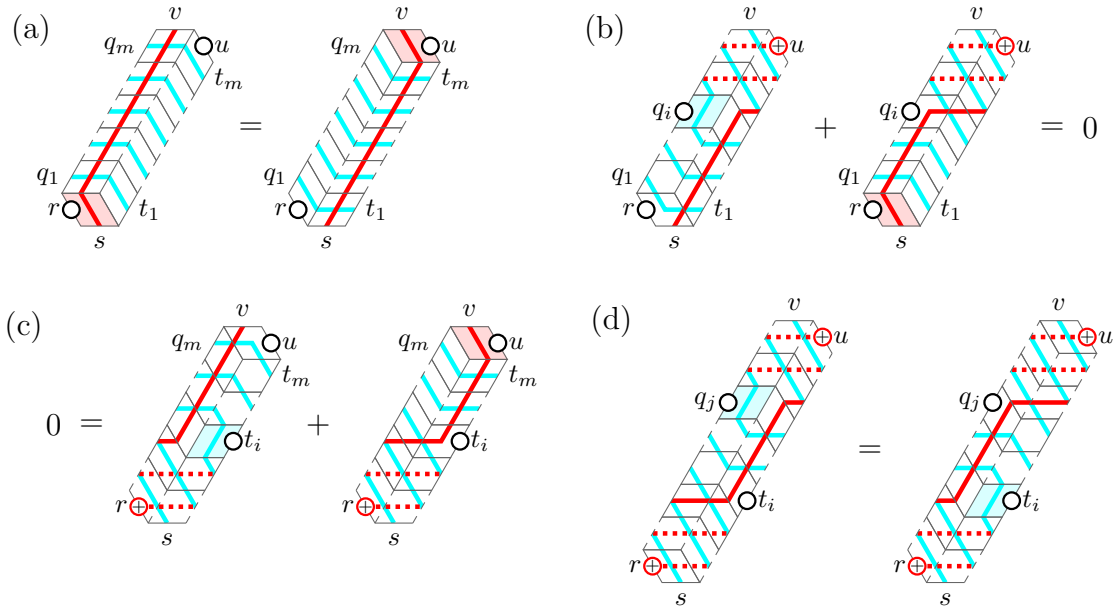
1. If there are $m-1$ separate blue lines, we have $q_i = 0$ for some $1 \leq i \leq m$. As argued in Lemma 5.18, we can assume $t_i, \ldots, t_m$ and $q_1, \ldots, q_{i-1}$ are nonzero and a blue line b entering at t_i must exit at q_{i-1}. If b crosses a blue line, we have at least m separate blue lines, so b crosses two red lines. These cases only use trivial tiles, covered by Lemma 5.15. We give a general outline where $1 \leq h < i \leq m$:



2. If there are $m+1$ separate blue lines, these cases only use trivial tiles and so are covered by Lemma 5.15:



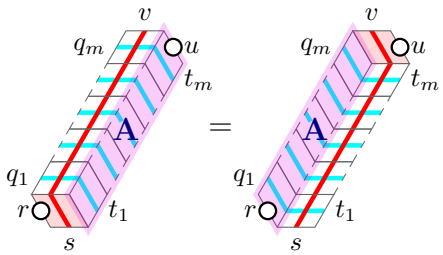
3. If there are m separate blue lines, there are four outlines using a nontrivial tile.



We expand on each case, as allowing crossings requires more careful analysis. Note that, in each case detailed below, the same crossings occur in each tiling, so we do not need to take into consideration the permutation σ. If σ does not allow these crossings, both sides of the equation are 0. If σ does allow these crossings, we might require more conditions on the lines.

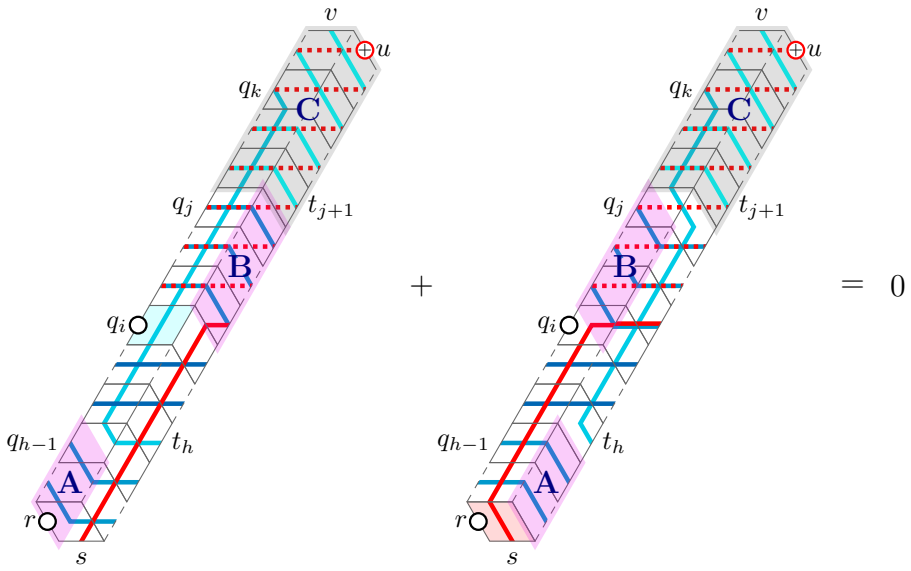
Case 3a:

In this case, regions both labelled **A** are decorated identically, no matter how the lines cross.



Case 3b:

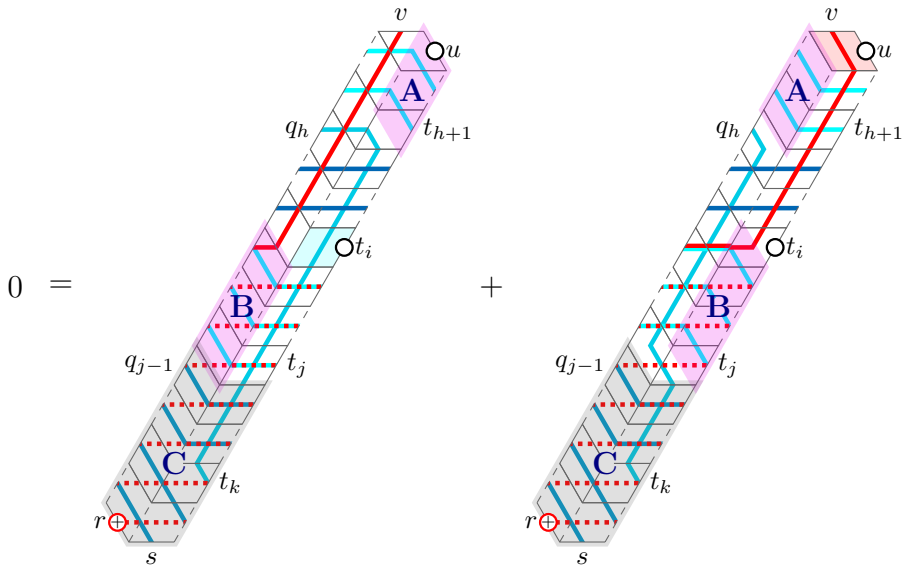
In this case, we track the blue line in the left tiling that crosses through a nontrivial tile with boundary label q_i. Say this line enters at t_h and exits at q_k. We allow $k = m + 1$, in which case we say $v = q_k$ and line t_h exits through the top at v. Let $1 \leq h \leq i \leq j < k \leq m + 1$. The most general situation is outlined below:



Regions both labelled **A**, **B** or **C** will be decorated identically. In both tilings, we must have $t_h \leq q_{h-1}$ or $h = 1$ and there will be no region **A**. If there exists some smallest value of j greater than i where either $\#(t_{j+1}) \leq t_h < \#(q_j)$ or $j = m$ and $t_h < \#(q_j)$, then there will be a region **B** as depicted; otherwise, **B** does not exist and we set $j = i$. When $j = m$, region **C** does not exist.

Case 3c:

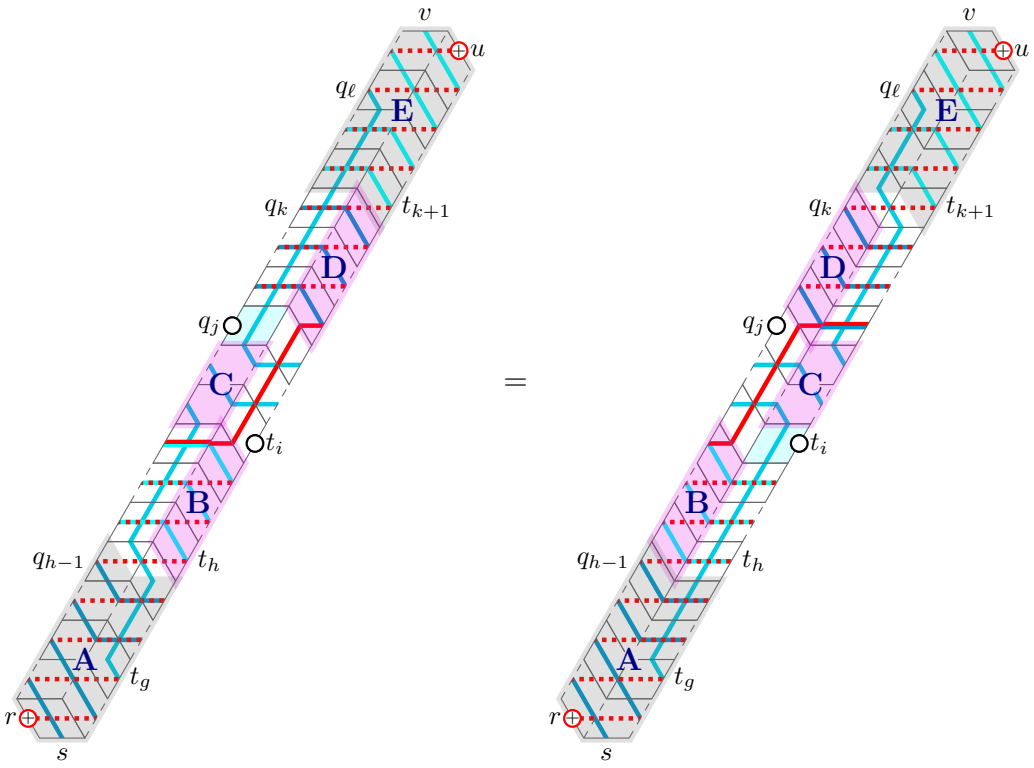
This case is very similar to 3b if it were rotated, though some care needs to be taken due to the asymmetry of the tiles under rotation. We track the blue line in the left tiling that crosses through a nontrivial tile with boundary label t_i. Say this line exits at q_h and enters at t_k. We allow $k = 0$, in which case we say $s = t_k$ and line q_h enters through the bottom at s. Let $0 \leq k < j \leq i \leq h \leq m$. The most general situation is outlined below:



Regions both labelled **A**, **B** or **C** will be decorated identically. In both tilings, we must have $t_{h+1} \leq q_h$ or $h = m$ and there will be no region **A**. If there exists some largest value of j less than i where either $\#(t_j) < q_h \leq \#(q_{j-1})$ or $j = 1$ and $\#(t_j) < q_h$, then there will be a region **B** as depicted; otherwise, **B** does not exist and we set $j = i$. When $j = 1$, region **C** does not exist.

Case 3d:

This case combines elements from 3b and 3c. We track the line that travels past q_j on the left-hand side of the equation (say it exits at q_ℓ) and the line that travels past t_i on the right-hand side (say it enters at t_g). Note that these may be the same line. If $g = 0$, say $t_g = s$ and line t_g enters through the bottom at s. If $\ell = m + 1$, say $q_\ell = v$ and line q_ℓ exits through the top at v. Let $0 \leq g < h \leq i < j \leq k < \ell \leq m+1$. The most general situation is outlined below:



Regions sharing labels **A** to **E** are identically decorated. We assume $i < j$, since $i = j$ is covered by Lemma 5.17; this entails that region **C** will always exist. The index h is the largest integer smaller than i where $\#(t_h) < \#(t_g) \leq \#(q_{h-1})$ or $h = 1$ and $\#(t_h) < \#(t_g)$; if no such index exists, then region **B** does not exist and we set $h = i$. The index k is the smallest integer larger than j where $\#(t_{k+1}) \leq \#(q_\ell) < \#(q_k)$ or $k = m$ and $\#(q_\ell) < \#(q_k)$; if no such k exists, region **D** does not exist and we set $k = j$. If $h = 1$, region **A** does not exist and if $k = m$, then region **E** does not exist.

□

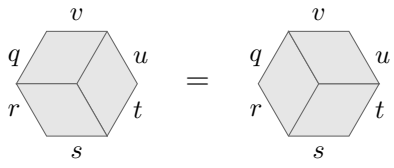
Chapter 6

Final Remarks

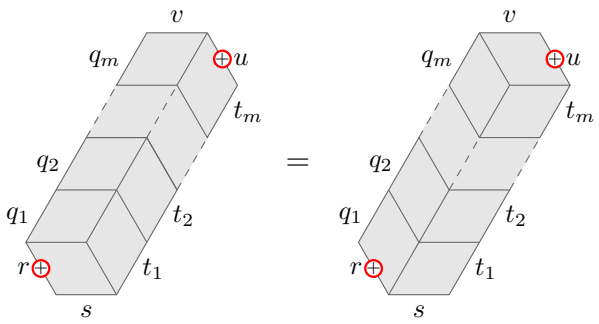
We conclude with final remarks. In Section 6.1, we comment on the peculiarity of our Yang–Baxter equation. Section 6.2 explains the issues with attempting this framework with "double" atoms, defined as a combinatorial analogue of double Schur polynomials. Finally, Section 6.3 suggests future directions to explore.

6.1 Comment on the Yang–Baxter equation

Zinn-Justin [50] and Wheeler and Zinn-Justin [48] had cleaner a Yang–Baxter equation that equates unit hexagons with unrestricted boundaries:



In contrast, our equation restricts the labels r and u on entire columns:



It is unclear if new tiles with new weights would permit a Yang–Baxter equation on unit hexagons with unrestricted boundaries, or if such an equation does not exist while also guaranteeing we compute the desired expansion. Adding new tiles so that the cases in Example 5.10 have matching pairs creates more issues, requiring more tiles, and creating new issues. This raises the question of whether such relaxations of the Yang–Baxter equation are a worthwhile area of exploration.

6.2 Equivariant tiles and double Demazure atoms

Double Schur polynomials $s_\lambda(\mathbf{x}|\mathbf{y})$ correspond to the equivariant cohomology of the Grassmannian. Zinn-Justin's original work in [50] computed the structure coefficients in the product of two double Schur polynomials:

$$s_\lambda(\mathbf{x}|\mathbf{z})s_\mu(\mathbf{x}|\mathbf{y}) = \sum_\nu e^\nu_{\lambda\mu}(\mathbf{y};\mathbf{z})s_\nu(\mathbf{x}|\mathbf{y}).$$

The model for double Schur polynomials is the same as the Schur model, only with the nontrivial tile given a weight of $x_c - y_r$ where c is the column number and r is the row number:

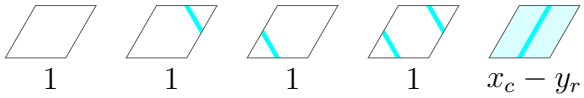


Figure 6.1: Tiles for the double Schur model.

Example 6.2. We have two fillings of the model for $s_\lambda(\mathbf{x}|\mathbf{y})$ when $\lambda = (2,1)$:



$(x_1 - y_1)(x_1 - y_3)(x_2 - y_1)$ $\qquad$ $(x_1 - y_1)(x_2 - y_1)(x_2 - y_2)$

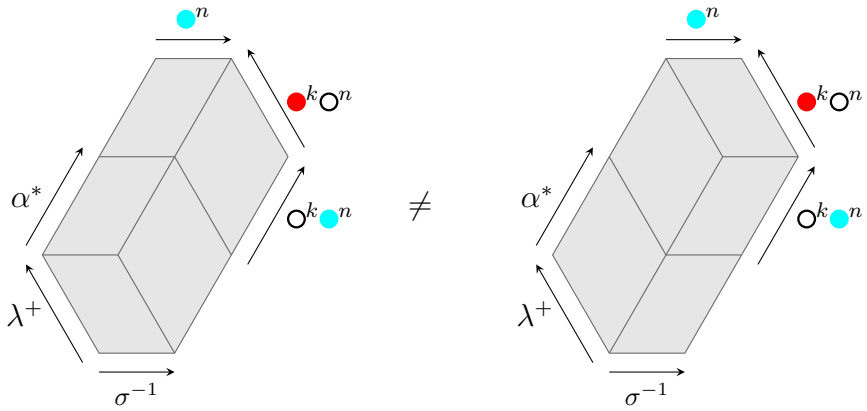
This computes that $s_\lambda(\mathbf{x}|\mathbf{y}) = (x_1 - y_1)(x_2 - y_1)(x_2 - y_2) + (x_1 - y_1)(x_1 - y_3)(x_2 - y_1)$.

The coefficients $e^\nu_{\lambda\mu}(\mathbf{y};\mathbf{z})$ are also computed with a diamond rule with one additional tile, which is called the equivariant tile because the expansion of double Schur polynomials corresponds to equivariant cohomology. The tile is assigned the weight $y_i - z_j$ where the indices i and j are determined by the tile's coordinates in the model:

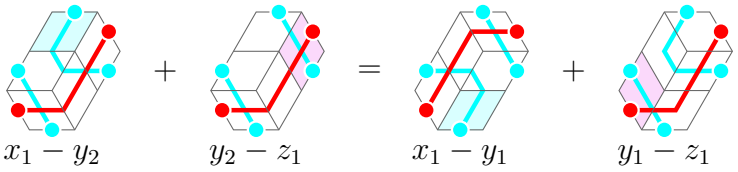


$y_i - z_j$

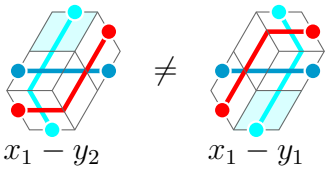
We can similarly allow the nontrivial weight $x_c - y_r$ in the atom model to create a combinatorial analogue of double Schur polynomials. However, we cannot run these through the same machinery to equate "prisms" as we do in Lemma 5.11. That is, we try reasonable rules incorporating new weights and the equivariant piece and have:



Essentially, there are issues with creating a column lemma with weights that track rows and columns. For instance, the equivariant tile in the product of two Schur polynomials allows for crucial cancellations. We display an example with weights as they could occur within a column. Both sides have weight $x_1 - z_1$:



Colouring this boundary differently and permitting crossings eliminates tilings that allow the cancellations:



Thus, we have not found a way to produce the product of a "double" atom with a double Schur polynomial. While the expansion proof may not work as desired, the "double" Demazure atoms may be an interesting area for future research.

6.3 Future directions

The K-theoretic analogues of Schur polynomials, Demazure atoms and Demazure characters are ***Stable Grothendieck polynomials*** $G_\lambda(\mathbf{x})$, ***Lascoux atoms*** $\overline{\mathcal{L}}_\alpha(\mathbf{x})$ and ***Lascoux polynomials*** $\mathcal{L}_\alpha(\mathbf{x})$, respectively. Wheeler and Zinn-Justin [48] have already extended the framework in [50] to stable Grothendieck polynomials. Further, Buciumas, Scrimshaw and Weber [13] have vertex models for Lascoux polynomials and atoms. Our results suggest these models could be combined in a similar way to yield the structure coefficients in the expansions of $\overline{\mathcal{L}}_\alpha(\mathbf{x})G_\lambda(\mathbf{x})$ and $\mathcal{L}_\alpha(\mathbf{x})G_\lambda(\mathbf{x})$. Orelowitz and Yu [42] have a tableau formula for the expansion of a Lascoux polynomial and a stable Grothendieck, but $\overline{\mathcal{L}}_\alpha(\mathbf{x})G_\lambda(\mathbf{x})$ remains unknown. One could also hope to define permuted-basement Lascoux atoms $\mathcal{L}^\sigma_\alpha(\mathbf{x})$ that specialize to Lascoux atoms and polynomials and prove all rules $\mathcal{L}^\sigma_\alpha(\mathbf{x})G_\lambda(\mathbf{x})$ simultaneously.

There are difficulties extending our approach to involve Bordin and Wheeler's full model for $E^{\sigma}_{\alpha}(\mathbf{x}; q, t)$ [8], as this model is on a cylinder and allows lines to wrap around; it is not clear how to address wrapping lines after gluing multiple models together. However, lines do not wrap around in the $q = 0$ case, so $E^{\sigma}_{\alpha}(\mathbf{x}; 0, t)$ might fit into this framework, possibly with new tiles and weights involving a t variable.

Demazure atoms and characters may be defined for other root systems, and so arises the question of other Cartan types. Our results are for atoms in type A, but Buciumas and Scrimshaw [12] have produced vertex models for Demazure atoms and Characters in types B and C. One could attempt to put these models within the structure coefficient framework, building on our results. The type B and C models have some profound difficulties arising from missing one of the four Yang–Baxter equations, but experimentation could yield a conjectural rule.

As mentioned in Section 1.3, it is a major open problem to show that the product of two characters $\mathcal{K}_{\alpha}(\mathbf{x})\mathcal{K}_{\beta}(\mathbf{x})$ has positive structure coefficients in the basis $\{\mathcal{A}_{\alpha}(\mathbf{x})\}_{\alpha}$. Our results were found while attempting to solve this problem, and we are now perhaps better situated to do so. It would also be interesting to explore our poset from Definition 2.10 in relation to this problem.

Vertex models also provide elegant frameworks for deriving Cauchy identities. It would be interesting to explore this framework for the following Cauchy identity [32], possibly incorporating permuted-basement versions:

$$\sum_{\alpha} \mathcal{K}_{\alpha}(\mathbf{x})\mathcal{A}_{\alpha}(\mathbf{y}) = \prod_{i+j \leq n} \frac{1}{1 - x_i y_i}.$$

References

[1] A. Aggarwal, A. Borodin, and M. Wheeler. Colored fermionic vertex models and symmetric functions. *Communications of the American Mathematical Society*, 3:400–630, 2023.

[2] P. Alexandersson. Non-symmetric Macdonald polynomials and Demazure–Lusztig operators. *Séminaire Lotharingien de Combinatoire*, 76, 2019. Article B76d, 27 pp.

[3] P. Alexandersson and M. Sawhney. Properties of non-symmetric Macdonald polynomials at $q = 1$ and $q = 0$. *Annals of Combinatorics*, 23:219–239, 2019.

[4] S. Assaf. An insertion algorithm for multiplying Demazure characters by Schur polynomials, 2023. arXiv:2109.05651.

[5] S. Assaf and D. Searles. Kohnert polynomials. *Experimental Mathematics*, 31(1):93–119, 2022.

[6] D. Betea and M. Wheeler. Refined Cauchy and Littlewood identities, plane partitions and symmetry classes of alternating sign matrices. *Journal of Combinatorial Theory, Series A*, 137:126–165, 2016.

[7] D. Betea, M. Wheeler, and P. Zinn-Justin. Refined Cauchy/Littlewood identities and six-vertex model partition functions: II. proofs and new conjectures. *Journal of Algebraic Combinatorics*, 42:555–603, 2015.

[8] A. Borodin and M. Wheeler. Nonsymmetric Macdonald polynomials via integrable vertex models. *Transactions of the American Mathematical Society*, 375:8353–8397, 2022.

[9] B. Brubaker, V. Buciumas, D. Bump, and H. P. A. Gustafsson. Colored five-vertex models and Demazure atoms. *Journal of Combinatorial Theory*, 178:159–195, 2021.

[10] B. Brubaker, C. Frechette, A. Hardt, E. Tibor, and K. Weber. Frozen pipes: lattice models for Grothendieck polynomials. *Algebraic Combinatorics*, 6(3):789–833, 2023.

[11] A. Buch, A. Kresch, K. Purbhoo, and H. Tamvakis. The puzzle conjecture for the cohomology of two-step flag manifolds. *Journal of Algebraic Combinatorics*, 44:973–1007, 2016.

[12] V. Buciumas and T. Scrimshaw. Quasi-solvable lattice models for Sp_{2n} and SO_{2n+1} Demazure atoms and characters. *Forum of Mathematics, Sigma*, 10, 2022. Article e53, 34 pp.

[13] V. Buciumas, T. Scrimshaw, and K. Weber. Colored five-vertex models and Lascoux polynomials and atoms. *Journal of the London Mathematical Society*, 102(3):1047–1066, 2020.

[14] I. Cherednik. Double affine Hecke algebras and Macdonald's conjectures. *Annals of Mathematics*, 141(1):191–216, 1995.

[15] I. Cherednik. Nonsymmetric Macdonald polynomials. *International Mathematics Research Notices*, 10:483–515, 1995.

[16] S. Corteel, A. Gitlin, D. Keating, and J. Meza. A vertex model for LLT polynomials. *Combinatorial Theory*, 2022(20):15869–15931, 2022.

[17] M. J. Curran, C. Frechette, C. Yost-Wolff, S. W. Zhang, and V. Zhang. A lattice model for super LLT polynomials. *Combinatorial Theory*, 3(2), 2023. Article #3, 52 pp.

[18] M. Demazure. Une nouvelle formule des caractères. *Bulletin des Sciences Mathématiques*, 98(3):163–172, 1974.

[19] E. Dimitrov. Six-vertex models and the GUE-corners process. *International Mathematics Research Notices*, 2020:1794–1881, 2020.

[20] J. P. Ferreira. *Row-strict quasisymmetric Schur functions, characterizations of Demazure atoms, and permuted basement nonsymmetric Macdonald polynomials*. PhD thesis, University of California Davis, 2011.

[21] A. Garbali and M. Wheeler. Modified Macdonald polynomials and integrability. *Communications in Mathematical Physics*, 374:1809–1876, 2020.

[22] A. Gunna and P. Zinn-Justin. Vertex models for canonical Grothendieck polynomials and their duals. *Algebraic Combinatorics*, 6:109–162, 2023.

[23] W. Guo and A. Ram. Comparing formulas for type GL_n Macdonald polynomials. *Algebraic Combinatorics*, 5(5):849–883, 2022.

[24] J. Haglund, M. Haiman, and N. Loehr. A combinatorial formula for nonsymmetric Macdonald polynomials. *American Journal of Mathematics*, 130:359–383, 2008.

[25] J. Haglund, K. Luoto, S. Mason, and S. van Willigenburg. Refinements of the Littlewood-Richardson rule. *Transactions of the American Mathematical Society*, 363(3):1665–1686, 2011.

[26] A. Knutson and K. Purbhoo. Product and puzzle formulae for gl_n Belkale-Kumar coefficients. *Electronic Journal of Combinatorics*, 18, 2011. Article #P76, 20 pp.

[27] A. Knutson and T. Tao. Puzzles and (equivariant) cohomology of Grassmannians. *Duke Mathematical Journal*, 119(2):221–260, 2003.

[28] A. Knutson, T. Tao, and C. Woodward. The honeycomb model of $GL_n(\mathbb{C})$ tensor products II: puzzles determine facets of the Littlewood-Richardson cone. *Journal of the American Mathematical Society*, 17(1):19–48, 2003.

[29] A. Knutson and P. Zinn-Justin. Schubert puzzles and integrability I: invariant trilinear forms, 2020. arXiv:1706.10019.

[30] A. Knutson and P. Zinn-Justin. Schubert puzzles and integrability II: multiplying motivic Segre classes, 2021. arXiv:2102.00563.

[31] A. Knutson and P. Zinn-Justin. Schubert puzzles and integrability III: separated descents, 2023. arXiv:2306.13855.

[32] A. Lascoux. Double crystal graphs. In *Studies in Memory of Issai Schur*, pages 95–114. Birkhäuser Boston, Boston, MA, 2003.

[33] A. Lascoux and M.-P. Schützenberger. Keys and standard bases. In *Invariant Theory and Tableaux (Minneapolis, MN, 1988)*, volume 19 of *IMA Volumes in Mathematics and its Applications*, pages 125–144. Springer, New York, 1990.

[34] D. E. Littlewood and A. R. Richardson. Group characters and algebra. *Philosophical Transactions of the Royal Society of London. Series A, Containing Papers of a Mathematical or Physical Character*, 233:99–141, 1934.

[35] I. G. Macdonald. Affine Hecke algebras and orthogonal polynomials. In *Séminaire Bourbaki : volume 1994/95, exposés 790-804*, number 237 in Astérisque, pages 189–207. Société mathématique de France, 1996. Exposé n° 797.

[36] S. Mason. A decomposition of Schur functions and an analogue of the Robinson–Schensted–Knuth algorithm. *Séminaire Lotharingien de Combinatoire*, 57, 2008. Article B57e, 24 pp.

[37] S. Mason. An explicit construction of type A Demazure atoms. *Journal of Algebraic Combinatorics*, 29:295–313, 2009.

[38] T. C. Miller. Vertex models for the product of a Schur and Demazure polynomial. *Séminaire Lotharingien de Combinatoire*, 91B, 2024. Article 100, 12 pp.

[39] T. C. Miller. Vertex models for the product of a permuted-basement Demazure atom and a Schur polynomial, 2025. arXiv:2503.09240.

[40] K. Motegi and K. Sakai. Vertex models, TASEP and Grothendieck polynomials. *Journal of Physics A: Mathematical and Theoretical*, 46(35), 2013. Article 355201, 26 pp.

[41] E. M. Opdam. Harmonic analysis for certain representations of graded Hecke algebras. *Acta Mathematica*, 175(1):75–121, 1995.

[42] G. Orelowitz and T. Yu. Lascoux expansion of the product of a Lascoux and a stable Grothendieck, 2023. arXiv:2312.01647.

[43] I. Pak and C. Robichaux. Signed puzzles for Schubert coefficients, 2025. arXiv:2504.17734.

[44] O. Pechenik and A. Yong. Equivariant K-theory of Grassmannians II: the Knutson–Vakil conjecture. *Compositio Mathematica*, 153:667–677, 2017.

[45] A. Pun. *On decomposition of the product of Demazure atoms and Demazure characters*. PhD thesis, University of Pennsylvania, 2016.

[46] D. Searles. Polynomial bases: positivity and Schur multiplication. *Transactions of the American Mathematical Society*, 373(2):819–847, 2020.

[47] M. Wheeler and P. Zinn-Justin. Refined Cauchy/Littlewood identities and six-vertex model partition functions: III. deformed bosons. *Advances in Mathematics*, 299:543–600, 2016.

[48] M. Wheeler and P. Zinn-Justin. Littlewood–Richardson coefficients for Grothendieck polynomials from integrability. *Journal für die Reine und Angewandte Mathematik*, 2019(757):159–195, 2019.

[49] C. Zhong. Stochastic symplectic ice. *Letters in Mathematical Physics*, 112, 2022. Article 55, 47 pp.

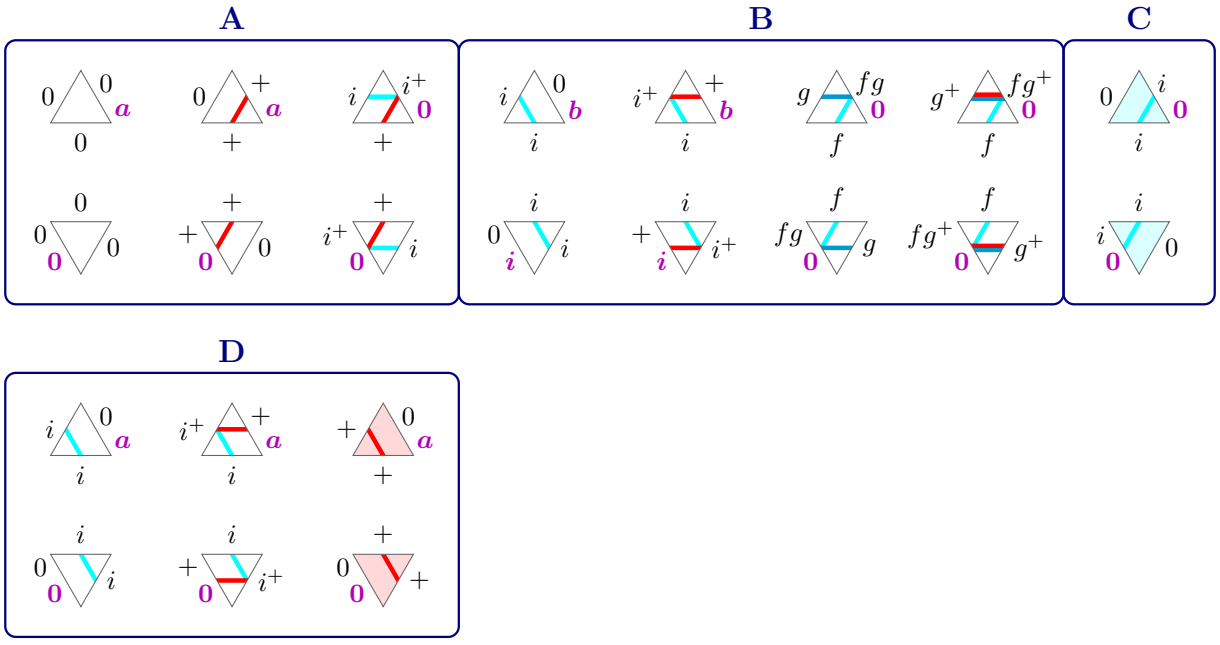
[50] P. Zinn-Justin. Littlewood–Richardson coefficients and integrable tilings. *Electronic Journal of Combinatorics*, 16(1), 2009. Article #R12, 33 pp.

APPENDICES

Appendix A

Triangle tiles and extra labels

We may add extra labels to our tiles in Figure 5.6 to enforce the restrictions in Figure 5.2 between diamond tiles, only requiring that labels match along edges. We construct rhombic tiles out of triangles with extra labels, emphasized in bold purple font.

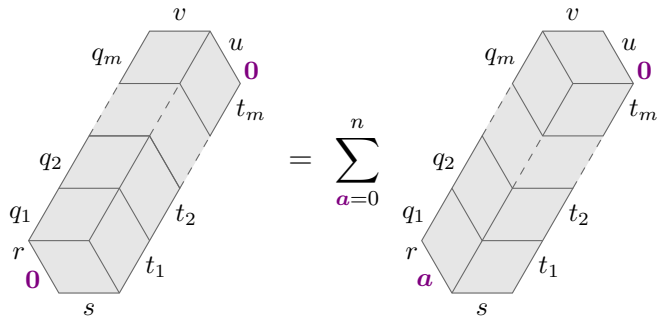


Here, $i, f, g \in [n]$, $\sigma(f) < \sigma(g)$, $0 \leq a \leq n$ and $0 \leq b \leq i$. Rhombic tiles only use a subset of triangular tiles, depending on the orientation of the rhombus. Pairs of triangles within

each subset are glued together in all possible ways, where labels match, producing rhombi of the corresponding orientation.

- Triangles **A** and **B** construct diamond tiles.
- Triangles **A**, **B** and **C** construct right-sheared tiles.
- Triangles **A** and **D** construct left-sheared tiles.

The resulting tiles are almost identical to Figure 5.6, only with two extra labels on the diamond and left-sheared tiles; right-sheared tiles are the same as before. However, this new labelling scheme implies we should adjust the Column Lemma 5.8 to sum over these new labels on the right-hand side, giving



where r and u are in $\{0, +\}$. The statement of Theorem 5.3 will also change, summing over all values of the extra labels along the southwest boundary and setting extra labels along the northeast boundary to 0.